Chapter 2

Transcritical refrigerating devices

2.1 Reasons of interest

Conventional modeling approaches remain confined in the characteristic dimensional scale of the final user, while the formulation of lower-scale models aims to complete the picture of the phenomenon by considering as many scales as possible in order to increase the accuracy and the suitability of the description. The result can be very far from the immediate sensitivity of the final user because it is usually much more complicated, but this does not mean that this description is less useful for the final design purposes. A simpler model can appear nicer but it will be less powerful in predicting something really new, which was not implicitly included in the averaged quantities considered as input data.

In the following, a particular technological application, i.e. the transcritical refrigerating plants with carbon dioxide as working fluid, will be considered. This application has been selected for the following reasons.

- First of all, the possibility of using again the carbon dioxide as working fluid in the refrigerating plants with performance which tries to approach that of usual devices based on synthetic fluids is chiefly due to a miniaturization process. In particular, this miniaturization process deals with the design of mini/micro channel compact heat exchangers and it can be considered a geometrical im-

provement, since no additional functional elements are added to these devices.

- Secondly, at this development stage, some uncertainties exist about the heat transfer properties of carbon dioxide and this will allow us to appreciate the effects of the lower scales. In fact, the peculiar phenomena, which rise close to the critical point, make it very difficult to obtain an accurate experimental measurement of the heat transfer parameters (*end-user* scale). This situation partially justifies the great discrepancies that exist among different phenomenological correlations, which have been proposed throughout the last years. In this case, to formulate a lower-scale model means to go back to more fundamental phenomena (*underlying* scale), which affect the heat transfer parameters, trying to obtain some additional information by directly modeling them.
- Finally, the permeation of carbon dioxide throughout the gaskets of the connecting components is a critical issue because of the high operating pressures; this undesired phenomenon allows us to appreciate the practical effects of modeling fluid flow in micro-structures.

This chapter is organized as follows. Some information about the history of carbon dioxide as refrigerant, its thermodynamic and thermo-physical properties and the specific issues of the consequent transcritical cycles are reported. The design of the experimental test rig and the results of the experimental plan are discussed. Finally, a reduced model fitting the previous experimental data is developed and some interpolating results are reported.

2.1.1 Trends of regulation on refrigeration technology

Over the last decades, the refrigeration, air conditioning and heat pump industry has been forced through major changes caused by restrictions on refrigerants. For

this reason, research and development in this field have been strongly influenced by environmental issues. These constraints are becoming more and more restrictive with respect to the utilization of synthetic fluids in the refrigeration technology. For this reason, some synthetic fluids that were once expected to be acceptable permanent replacement fluids are now on the list of regulated substances due to their impact on the environment. The present refrigeration technology, and even more the future one, will not be allowed to develop devices without taking care of the effects on the global environment.

Essentially the great majority of the synthetic fluids which have been developed for the refrigeration technology derive from paraffinic hydrocarbons and they can be obtained by substituting the hydrogen atoms with atoms of other substances, like chlorine and fluorine. Depending on the final result of this process, the synthetic fluids can be subdivided in three categories:

- the chlorofluorocarbons (CFCs), which are the compounds made from carbon, chlorine and fluorine;
- the hydrochlorofluorocarbons ($HCFC$s), which are the compounds made from carbon, hydrogen, fluorine and chlorine;
- the hydrofluorocarbons (HFCs), which are the compounds made from carbon, hydrogen and fluorine.

Some widespread synthetic fluids and some natural fluids used in the refrigeration technology are reported in Tab. 2.1.

All the regulations for refrigeration technology refer to some indexes, which allow us to quantify the effects of the synthetic substances on the global environment. The two most serious effects of the human activity on the global environment concern

Table 2.1: Some widespread synthetic fluids and some natural fluids in refrigeration technology (ASHRAE codes are adopted).

	Chlorofluorocarbons (CFCs)	
ASHRAE Code	Chemical Formula	Chemical Name
R-11	$C\,Cl_3\,F$	Trichlorofluoromethane
R-113	$C\,Cl_2\,F\,C\,Cl\,F_2$	Trichlorotrifluoroethane
R-114	$C\,Cl\,F_2\,C\,Cl\,F_2$	Dichlorotetrafluoroethane
R-12	$C\,Cl_2\,F_2$	Dichlorodifluoromethane
R-13	$C\,Cl\,F_3$	Chlorotrifluoromethane
R-14	$C\,F_4$	Tetrafluoromethane
R-C318	$C_4\,F_8$	Octafluorocyclebutane
	Hydrochlorofluorocarbons ($HCFC$s)	
R-123	$C\,H\,Cl_2\,C\,F_3$	Dichlorotrifluoroethane
R-21	$C\,H\,Cl_2\,F$	Dichlorofluoromethane
R-22	$C\,H\,Cl\,F_2$	Chlorodifluoromethane
	Hydrofluorocarbons (HFCs)	
R-134a	$C\,H_2\,F\,C\,F_3$	1,1,1,2-tetrafluoroethane
R-152	$C\,H_3\,C\,H\,F_2$	1,1-difluoroethane
R-23	$C\,H\,F_3$	Trifluoromethane
	Mixtures	
R-401A	R-22/152a/124 (53/13/34)	Ternary mixture
R-407C	R-32/125/134a (23/25/52)	Ternary mixture
R-410A	R-32/125 (50/50)	Binary mixture
R-507	R-125/143a (50/50)	Binary mixture
	Natural Fluids	
R-1150	$C\,H_2 = C\,H_2$	Ethene (ethylene)
R-1270	$C\,H_3\,C\,H = C\,H_2$	Propene (propylene)
R-170	$C\,H_3\,C\,H_3$	Ethane
R-290	$C\,H_3\,C\,H_2\,C\,H_3$	Propane
R-50	$C\,H_4$	Methane
R-600	$C\,H_3\,C\,H_2\,C\,H_2\,C\,H_3$	Butane
R-600a	$C\,H\,(C\,H_3)_3$	2-methyl propane (isobutane)
R-717	$N\,H_3$	Ammonia
R-718	$H_2\,O$	Water
R-728	N_2	Nitrogen
R-729	$N_2/O_2/A$ (76/23/1)	Air
R-732	O_2	Oxygen
R-740	A	Argon
R-744	$C\,O_2$	Carbon dioxide

the anthropic (or enhanced) global warming due to the greenhouse effect and the depletion of the stratospheric ozone layer.

The greenhouse effect is a naturally occurring process that aids in heating the Earth's surface and atmosphere. It results from the fact that certain atmospheric gases, such as carbon dioxide, water vapor, and methane, are able to change the energy balance of the Earth by being able to absorb relatively long-wave radiation from the Earth's surface. These gases are called greenhouse gases. Without the greenhouse effect, life on this planet would probably not exist as the average temperature of the Earth would be too low. The relevance of this effect is controlled by the concentration of greenhouse gases in the Earth's atmosphere. All of the major greenhouse gases have increased in concentration since the beginning of the industrial revolution. Some evidences exist which seem to suggest that a result of these higher concentrations is an enhanced global warming which could affect the planet climate. The most common greenhouse gases include: carbon dioxide (CO_2); methane (CH_4); nitrous oxide (N_2O); the synthetic fluids involved in the refrigeration technology (CFCs, $HCFC$s and HFCs); and tropospheric ozone (0_3). Even though the synthetic fluids involved in the refrigeration technology are the strongest greenhouse gases per molecule, they account for the 25% of the change in the intensity of the Earth's greenhouse effect, i.e. less than the contribution due to the carbon dioxide which accounts for the 50%.

In order to estimate the effects of a chemical substance with regard to the anthropic global warning, the global warming potential (GWP) may be considered. This index relates the potential of a greenhouse gas to that of carbon dioxide over a 100-year period and it is determinated by the Intergovernmental Panel on Climate Change. The synthetic fluids created for the refrigeration technology are characterized by GWPs which are three orders of magnitude higher than the GWP of carbon dioxide,

which has $GWP = 1$ by definition. Another very popular index is the total equivalent warming impact, $TEWI$, used to measure the overall contribution of a technology to global warming. This index is slightly less rigorous than the previous one because it depends as well on the considered technology which uses the fluid and the installation location of the device but it still gives good relative comparisons. The $TEWI$ index takes into account the whole life cycle of the considered device and the indirect effects on the global environment in order to allow proper device operation. This is important for comparison involving synthetic fluids and natural fluids, because the natural fluids usually imply lower efficiency since they are not designed for any specific application. Since the synthetic fluids involved in refrigeration have some effects on the enhanced global warming, they are included in the Kyoto Protocol. The Kyoto Protocol has been defined by the United Nations Framework Convention on Climate Change during the world conference at Kyoto (Japan) in 1997, in order to reduce the anthropogenic carbon dioxide equivalent emissions of greenhouse gases. The Kyoto Protocol is not yet in force since the number of countries that have ratified it is not sufficient, but the general trends which inspire this protocol are widely shared and they will affect the technological development whether it will be ratified or not.

While the synthetic fluids for refrigeration are not the leading causes of the enhanced global warming, the situation is completely different if the depletion of the stratospheric ozone layer is considered. The ozone layer is a region of concentration of the O_3 molecule in the Earth's atmosphere. The layer sits at an altitude of about 10-50 km, with a maximum concentration in the stratosphere at an altitude of 25 km. In recent years, some evidences exist that the stratospheric ozone layer is becoming thinner, primarily at the poles, and this phenomenon is being called the ozone hole. The ozone layer naturally shields Earth's life from the harmful effects

of the solar ultraviolet radiation. A severe decrease in the concentration of ozone in the ozone layer could lead to harmful effects, like an increase in the number of cases of skin cancer, a sharp increase in cataracts and sun burning, suppression of immune systems and a reduction in the growth of ocean phytoplankton. The ozone layer is naturally produced by the solar ultraviolet radiation which hits the stratosphere. The CFCs, and secondly the $HCFC$s, created at the Earth's surface slowly drift upward to the stratosphere where ultraviolet radiation from the sun causes their decomposition and the release of chlorine. Chlorine in turn attacks the molecules of ozone converting them into oxygen molecules. The human activities are altering the amount of stratospheric ozone, with the main culprits being human-made CFCs and $HCFC$s.

The ozone depletion potential (ODP) is a measure of the ability of a compound to reduce the amount of stratospheric ozone and it can be used to quantify the effects of a chemical substance on the global environment. The ODP is the technical tool adopted by the Montreal Protocol and it is defined as the ratio of calculated ozone column change for each mass unit of a gas emitted into the atmosphere relative to the calculated depletion for a reference gas (R-11). The Montreal Protocol is the first worldwide agreement designed to protect human health and the environment against the adverse effects of the depletion of the stratospheric ozone layer. The protocol is administered by the United Nations Environment Program, which maintains the list of ozone-depleting substances that are targeted for control practices, reductions, or total phase-outs. The ODP formed the primary basis for inclusion on the list, although the final list was a product of international negotiation. The Montreal Protocol divides ozone depleting substances into a variety of lists of chemicals that are subject to different control requirements. Countries that signed the treaty committed

to:

1. reduce consumption or production of $HCFC$s to 1989 levels;
2. stop consumption or production of chemicals on Group 2 after January 1^{st}, 1994 ($Halon$ 1211, $Halon$ 1301, and $Halon$ 2402);
3. stop consumption or production of chemicals on Group 1 after January 1^{st}, 1996 (R-11, R-12, R-113, R-114, and R-115);
4. stop consumption or production of chemicals on Groups 1, 2 and 3 after January 1^{st}, 1996 (R-13, R-111, R-112, R-211, R-212, R-213, R-214, R-215, R-216, R-217, carbon tetrachloride, and 1,1,1-trichloroethane);
5. reduce consumption or production of methyl bromide to 75% of 1991 levels beginning in 1999.

The Montreal Protocol mandated an end to the production and consumption of the major CFCs, halons, hydrobromofluorocarbons ($HBFC$s) and methyl bromide by 1996, while the $HCFC$s are tolerated but they are not considered acceptable permanent replacement fluids. Implementation of the Montreal Protocol was dependent on national regulation. In particular, the European Union (EU) regulation on ozone depleting substances, EU 2037/2000 applies from October 1^{st} 2000, upon which date the previous regulation, EU 3093/94, was repealed. The remarkable feature of this EU regulation is that in some cases it goes beyond the requirements of the Montreal Protocol, particularly with regard to the $HCFC$s. The key points are discussed in the following.

- New bans on the supply and use of CFCs, $Halons$, 1,1,1-trichloroethane, carbon tetrachloride, $HBFC$s and bromochloromethane. These bans apply from October 1^{st} 2000 for most applications, although certain delays and exceptions apply. The bans on these substances apply to both virgin and recycled material.

- Significant revisions to the control on use of $HCFC$s. This adds a number of new controls to those specified in the previous EU regulation. $HCFC$s will not be allowed to be used in new equipment from January 1^{st} 2001 (with some exemptions) and servicing $HCFC$ systems will be restricted to the use of recovered/reclaimed refrigerant from January 1^{st} 2010 to December 31^{st} 2014. All the major end use sectors for $HCFC$s are subject to new use controls.

- Tougher requirements regarding the recovery of ozone depleting substances from products and equipment and to prevent leakage from systems.

- A ban on the supply of ozone depleting substances in disposable containers (except for essential uses).

- A revised timetable for the supply of $HCFC$s. The timetable was designed to match the new HCFC end use controls. Some cuts came into effect in 2001 and there was a substantial cut by 2003. No virgin $HCFC$s can be supplied after the end of 2009.

- A ban on the import of products containing ozone depleting substances. This is immediate for all ozone depleting substances except $HCFC$s, which are characterized by specific use control dates.

- A ban on the export of virgin and recycled CFCs and $Halons$ and products containing them, although certain exemptions apply.

- A new timetable for the phase out of EU production of $HCFC$s.

A complete discussion about the regulation on this subject is beyond the purposes of the present work. It is important to point out that, in the international regulation, an unquestionable trend exists, which aims to reduce and eventually eliminate the

utilization of synthetic fluids in refrigeration technology. The consecutive regulations on this subject become more and more restrictive and they implicitly suggest to move to natural fluids in order to find different long-term solutions. Instead of continuing the search for new chemicals, there is an increasing interest in technology based on ecologically safe refrigerants, i.e. fluids like water, air, noble gases, hydrocarbons, ammonia and carbon dioxide [20].

2.1.2 Recovery of natural fluids

The ASHRAE (American Society of Heating, Refrigerating and Air-Conditioning Engineers) has set more than two thousand fluids theoretically suitable as working fluids for vapor compression. Just a few of the proposed ones are natural, i.e. are naturally present in the Earth biosphere. As outlined in the previous section, environmental problems have gained increasing importance and they suggest a recovery of natural fluids. The possible natural fluids which could be used in refrigeration based on vapor compression are:

- ammonia (R-717);
- hydrocarbons (mainly isobutane R-600a and propane R-290);
- carbon dioxide (R-744);
- air (R-729);
- argon (R-740).

The most important characteristics of these fluids are reported in Tab. 2.2. The usual operating temperatures for vapor cycles in air conditioning systems are included between 0 $^{\circ}C$ and +50 $^{\circ}C$. In this range of temperature, air and argon are present only as in the gas state, as it is easy to verify by considering the critical point, and for this reason those fluids have not been included in Tab. 2.2. It must be pointed out

Table 2.2: Comparison among some synthetic and natural refrigerants (source [20]).

	R-12	*R*-22	*R*-134*a*	*R*-407*C*	*R*-410*A*	*R*-717	*R*-600*a*	*R*-290	*R*-744
OPD/GWP[a]	1/8500	0.05/1700	0/1300	0/1600	0/1900	0/0	0/20	0/3	0/1
Flammability / Toxicity	N/N	N/N	N/N	N/N	N/N	Y/Y	Y/N	Y/N	N/N
Molecular mass $[kg/kmol]$	120.9	86.5	102.0	86.2	72.6	17.0	58.1	44.1	44.0
Normal boiling point[b] $[\mathcal{C}]$	-29.8	-40.8	-26.2	-43.8	-52.6	-33.3	-11.6	-42.1	-78.4
Critical pressure $[MPa]$	4.11	4.97	4.07	4.64	4.79	11.42	3.64	4.25	7.48
Critical temperature $[\mathcal{C}]$	112.0	96.0	101.1	86.1	70.2	133.0	134.7	96.7	31.1
Reduced pressure[c] $[-]$	0.07	0.10	0.07	0.11	0.16	0.04	0.04	0.11	0.47
Reduced temperature[d] $[-]$	0.71	0.74	0.73	0.76	0.79	0.67	0.67	0.74	0.90
Refrigeration capacity[e] $[kJ/m^3]$	2734	4356	2868	4029	6763	4382	1509	3907	22545
First commercial use as refrigerant	1931	1936	1990	1998	1998	1859	?	?	1869

[a] Global warming potential in relation to 100 years integration time, from the Intergovernmental Panel on Climate Change (IPCC).
[b] ASHRAE handbook 2001 fundamentals.
[c] Ratio of saturation pressure at $273.15\,K$ to critical pressure.
[d] Ratio of $273.15\,K$ to critical temperature.
[e] Volumetric refrigeration capacity at $273.15\,K$.

that carbon dioxide, due to its critical temperature 31.1 $℃$, realizes a transcritical cycle for the considered operating conditions, that is a refrigerating cycle that works between two different pressures: evaporating pressure below the critical one and the heat rejection pressure above. All the other fluids are characterized by the usual configuration and phase-change processes exist for both operating pressures.

A complete review of all refrigeration systems where natural fluids can be suitability adopted and a serious comparison among possible natural candidates according to the considered application is beyond the purposes of the present work. Some good reviews about this subject may be considered [22, 23]. In order to compare the suitability of the considered natural fluids for air conditioning applications, only some essential features will be discussed [21].

1. *Working pressure*

   The operating pressures for R-717 and R-290 are very similar, while the R-600a is characterized by lower values and R-744 is characterized by much greater pressures. Increasing the operating pressure of the working fluid is usually considered a difficulty and for this reason the previous comparison seems to be unfavorable to carbon dioxide. However it must be pointed out that high working pressure fluids are less penalized than lower pressure fluids when taking into account temperature drops related to pressure drops, being the same the crossing velocity. For this reason, we can increase the crossing velocity inside heat exchangers obtaining higher heat transfer coefficients, and so a better efficiency in the heat transfer process.

   The worry about carbon dioxide high working pressures is not justified if we consider that its volumetric latent heat is higher than that of all other natural fluids. A large value of volumetric latent heat implies a reduction of the volume

flow rate to be run to obtain the same refrigeration capacity. High operating pressure and the related high vapor density make it possible to employ small size piping and heat exchangers with small internal volume. For this reason the danger linked to a possible explosion is small because this danger is related to the mechanical energy inside the circuit, which is proportional to volume. For the same reason, carbon dioxide implies a reduction of the refrigerant charge and consequently more compact compressors and lighter machines. The last feature is particularly relevant for airborne systems, as will be discussed later on.

Even though the carbon dioxide high working pressures do not imply a real explosion danger, they may induce some leakage problems. Since carbon dioxide is a natural fluid, possible leakages do not affect the environment but they usually hinder the thermodynamic performance of the systems. This problem may be reduced by considering special stainless steel connections. However cost reduction suggests to consider connecting components made of elastomers. Unfortunately the thermodynamic properties of carbon dioxide cause a high solubility as well as a moderate diffusion velocity in elastomers. For this reason, compared to other natural gases, the permeation rate results significantly higher. Special care must be taken in order to ensure acceptable performances during operating conditions. This feature will be further discussed at the end of Chapter 5.

2. *Heat transfer performance*

Considering the attitude to exchange heat, the worst among the selected natural fluids previously considered is isobutane (R-600a). This can be seen from the low thermal conductivity of the liquid and mainly the values of the vapor den-

sity and pressure. Propane and ammonia behave better. Indeed, carbon dioxide shows the best heat transfer performance. In the usual operative conditions for the working fluid in refrigerating machines and heat pumps, the thermophysical properties of carbon dioxide are favorable to produce high heat transfer coefficients in the heat exchangers of the equipment (of suitable geometry), often higher than those commonly obtained with traditional synthetic refrigerants.

3. *Compatibility with other materials*

   Ammonia is the worst natural fluid with regard to corrosion problems. In fact, the refrigerating plants based on ammonia as working fluid should involve steel or aluminum components, instead of copper in order to avoid corrosion problems. For the same reason, only few hermetic compressors exist for this fluid. Ammonia is virtually insoluble in the most commonly used lubricating oils.

   On the other hand, hydrocarbons and carbon dioxide do not display drawbacks in this respect and are compatible with common materials and oils. In particular, carbon dioxide is an inert product and is compatible with all common materials encountered in a refrigeration circuit, both metals and plastics or elastomers.

4. *Safety*

   Ammonia is toxic and the effects due to direct exposure can vary from eyes irritation up to death according to considered concentrations. Moreover, ammonia is flammable in air and this induces to avoid any possibility of direct contact between the circuit containing ammonia and the air to be distributed into conditioned space.

Hydrocarbons are not toxic, but they are flammable and for this reason they need safety constraints too. Some evidences exist that, in systems based on hydrocarbons, small refrigerant leakage in a confined space can easily provoke fire or explosions. Many markets in the world are quite restrictive to application of hydrocarbons in vapor compression systems. Even though the car air conditioning devices using hydrocarbons are allowed in Australia, the regulation on this subject is very severe.

Finally, carbon dioxide is a product that displays no special local safety problem, as it is non-flammable and non-toxic. However it is a gas heavier than air, it can accumulate in the lower part of a non-ventilated ambient, causing suffocation for lack of oxygen.

The introduction of natural refrigerants requires the development of improved technology in processes and components suitably adapted to their positive and negative characteristics, and the formulation of safety codes of practice and standards for systems and component design, installation and operation [24]. In particular, for ammonia and hydrocarbon applications there is a great need for uniform international regulations and standards based on accepted quantitative risk assessment studies. However, the possible widespread diffusion of ammonia and hydrocarbons seems a distant possibility in Europe and in U.S.A., with the exception of few applications which include supermarkets and domestic refrigerators respectively. Even though research on alternative refrigerants is continuing on many parallel paths, carbon dioxide is a very promising working fluid for vapor compression refrigerating systems.

Recent researches on transcritical carbon dioxide systems have investigated a variety of possible applications, which can make suitable use of the thermo-physical (thermodynamic and transport) properties of this natural fluid. For several reasons,

mobile air conditioning applications were among the first to be considered [20]. In particular, the automotive air conditioning sector yields many research programs, mostly with funding from involved industries [25–27]. In automobiles, a natural fluid for refrigerating systems would allow us to avoid any future regulation constraints due to the high leakage rates which characterize this application. Moreover, the high temperature of heat rejection allows us to design ultra-compact gas coolers, which increase energy efficiency and reduce the packaging problems due to integration with other subsystems in closed spaces (under-hood space management). Finally, the carbon dioxide is particularly suitable for working in heating mode and this can allow us to keep cars comfortable in severe winter conditions, when waste heat rejected by engine coolant is not enough.

Some of the previous considerations are not exclusive advantages for automotive application. In particular, lightweight and ultra-compact systems are highly valued by any mobile application. In this work, the airborne application will be considered. The present air conditioning systems for civil aircrafts are based on simple expansion of compressed air taken from engines and this implies very low efficiencies. In this case, a natural fluid (air) is already adopted but the possibility to consider a vapor compression system would enable to improve the efficiencies up to one order of magnitude in comparison with present devices. Obviously a vapor compression system requires an auxiliary electrical supply but this would be harmonious with new trends for new aircrafts which aim to decouple the auxiliaries from the propulsion power need. Despite previous considerations, the research in this field is still very poor. In the next section, the considered application will be discussed in a more detailed way in order to appreciate the most relevant topics and the specific features which may suggest to consider the transcritical refrigerating cycles.

2.1.3 Air-conditioning in airborne systems

In the aircraft industry, the term Environmental Control System (ECS) is used to identify the devices which allow us to realize suitable environmental conditions for passengers and crew inside the cabin. ECS includes systems and equipment associated with the ventilation, heating, cooling, humidity/contamination control and pressurization in the passenger and cargo compartments, and the electronic equipment bays [28]. Environmental control systems of various type and complexity are used in military and civil aircraft, helicopter and spacecraft applications. In the following, only commercial transport aircraft will be considered. For this market application, air-cycle air conditioning for the ECS represents the largely predominant strategy. The Brayton refrigeration cycle is preferred to the Evans-Perkins cycle. This strategy is usually a matter of convenience due to the easiness of extracting compressed air from engine bleeds but it enormously increases the energy consumption for air-conditioning.

Two features are the most distinguishing for the present application. Aircraft ECSs operate under very extreme conditions because the external physical environment during flight conditions is not survivable by unprotected humans. Outside air at cruise altitude is extremely cold, dry and can contain high levels of ozone. On the other hand, while on the ground air can be hot, humid, and contain many pollutants, such as particulate matter, aerosols and hydrocarbons. These ambient conditions change quickly from ground operations to flight. In addition to essential safety requirements, the ECS should provide a comfortable environment for the passengers and the crew. This is complicated by the high seating density of the passengers, the changes in cabin pressure and the changes of outside environment during flight.

First of all, let us consider an usual ECS based on air-cycle refrigeration system.

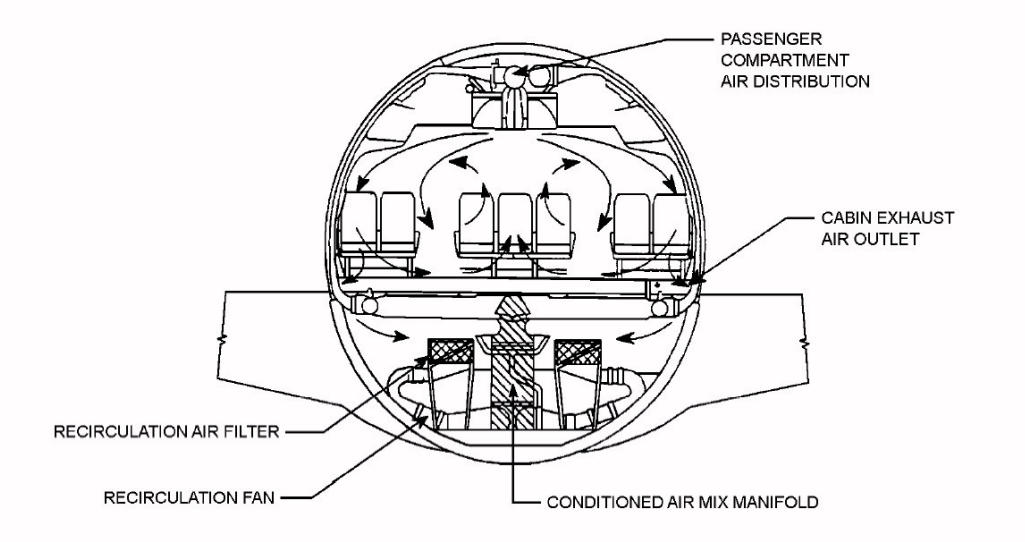

Figure 2.1: Cabin airflow patters [28, 29].

The outside air supplied to the airplane cabin is provided by the engine compressors, cooled by air-conditioning packs located under the wing center section and mixed with an equal quantity of filtered, recirculated air. As shown in Fig. 2.1, air enters the passenger cabin from overhead distribution outlets that run the length of the cabin. The exhaust air leaves the cabin through return air grilles located in the sidewalls near the floor and running the length of the cabin on the both sides. The cabin ventilation is designed and balanced so that air supplied at one seat row leaves at approximately the same seat row, thus minimizing airflow in the cabin. The following basic systems comprise the typical aircraft ECS based on air-cycle refrigeration cycle [28].

1. *Pneumatic system*

   The pneumatic system or engine bleed air system extracts a small amount of air from the engine compressor to ventilate and pressurize the aircraft compartments. A schematic of a typical engine bleed air system is shown in Fig. 2.2. Essentially four ports are available in order to extract engine compressed air, characterized by increasing pressure levels: starter, fan, intermediate pressure

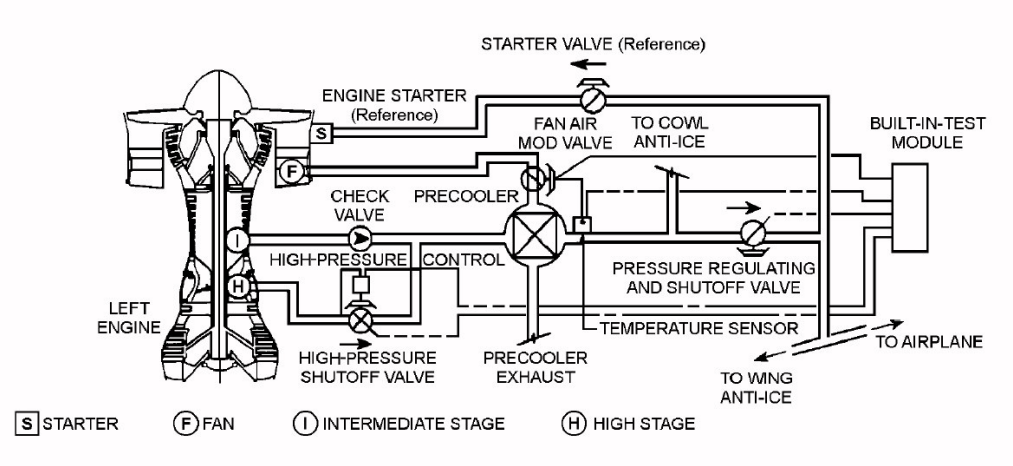

Figure 2.2: Typical engine bleed air system schematic [28, 29].

and high pressure port. During climb and cruise, the bleed air is usually taken from the intermediate pressure port for minimum bleed penalty. During idle descent, it is taken from the high pressure port where maximum available pressure is required to maintain cabin pressure and ventilation. Air extracted from the fan port can be used as the heat sink for the bleed air heat exchanger (precooler), or ram port can be used (see Fig. 2.2), which usually requires an ejector or fan for static operation.

2. *Air-conditioning system*

The Air Cycle System (ACS) realizes the requested cooling capacity by means of a Brayton inverse cycle. Essentially this process can be realized in three steps. Ambient air compressed by the engine compressor provides the power input, the heat of compression is removed in a heat exchanger using ambient air as heat sink and finally the cooled air is refrigerated by expansion across a turbine. The turbine energy resulting from expansion is absorbed by an auxiliary machine, which is either a ram air fan, a further bleed air compressor or both [28]. This

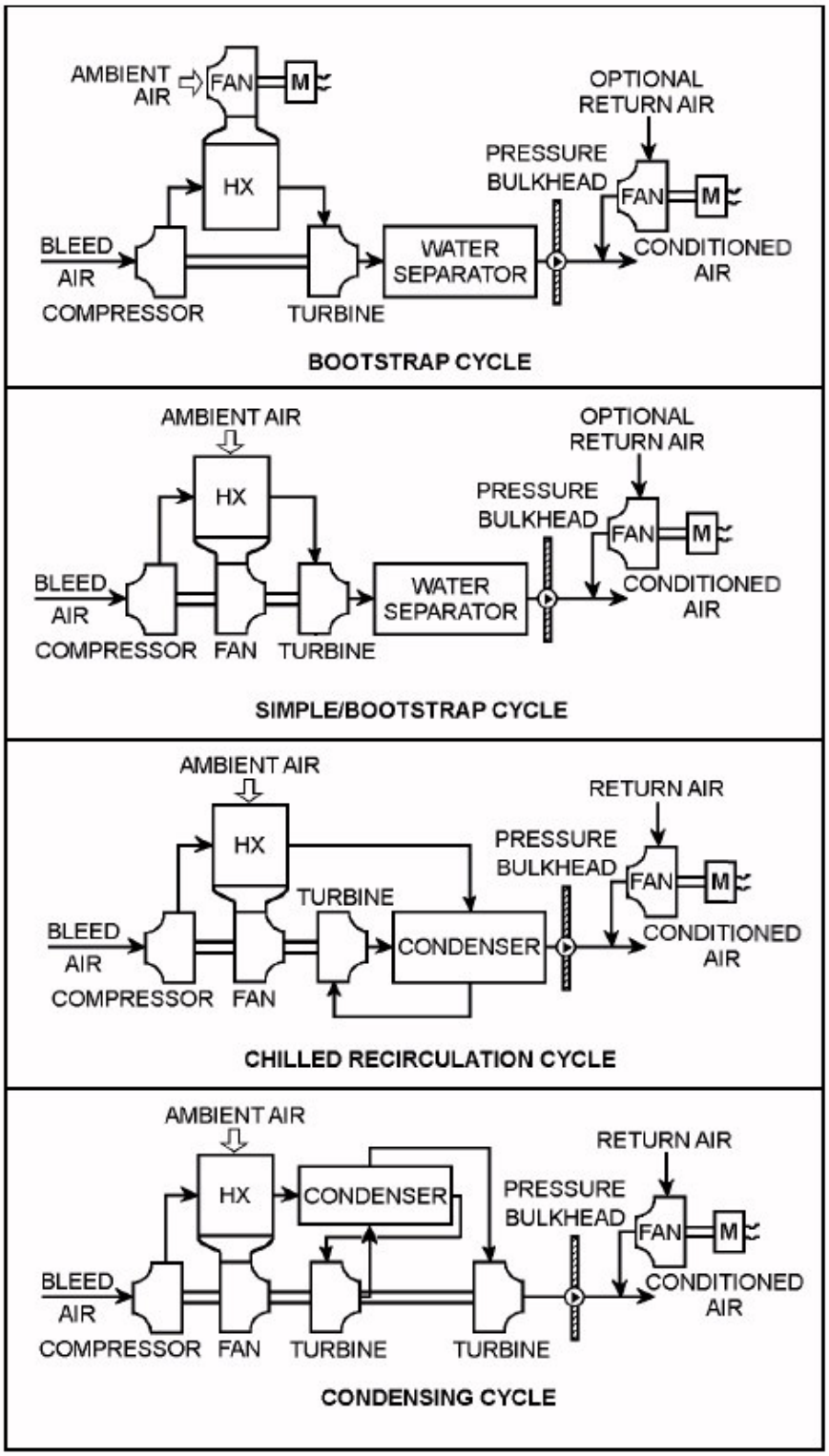

Figure 2.3: Typical air cycle systems (ACSs) [28, 29].

assembly is called an air cycle system (ACS). Moisture condensed during the refrigeration process is removed by a water separator.

The most common types of air-conditioning cycles in use on commercial transport aircraft are shown in Fig. 2.3. The most used air-cycle machines are:

- the (two-wheel) bootstrap ACS consisting of a turbine and an auxiliary compressor which further compresses the bleeded air;
- the three-wheel ACS consisting of a turbine, an auxiliary compressor and a fan which moves the ambient air needed for cooling the compressed air before expansion (3WM-ACS);
- the four-wheel ACS consisting of two turbines which allow intermediate removal of the moisture, an auxiliary compressor and a fan.

The three-wheel ACS is used on most of the newer commercial aircrafts, including commuter aircrafts and business aircrafts. The four-wheel ACS was first applied on the Boeing 777 aircraft and it is still used today.

3. *Cabin pressure controller*

   Cabin pressure is controlled by modulating the airflow discharged from the pressurized cabin through one or more cabin outflow valves. The system controls the cabin ascent and descent rates to acceptable comfort levels and maintains cabin pressure altitude in accordance with cabin-to-ambient differential pressure schedules.

This traditional picture of the ECS is nowadays under discussion. In fact the goal of reducing energy consumption due to transportation is considered a top priority issue and it will affect the aircraft industries in the next years by forcing the development

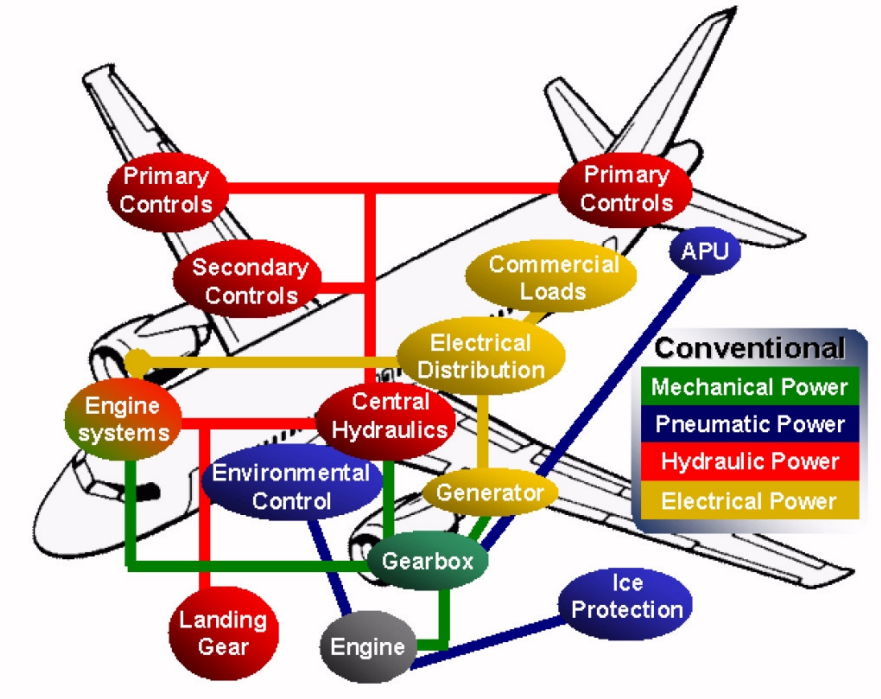

Figure 2.4: Schematic of conventional power distribution [31].

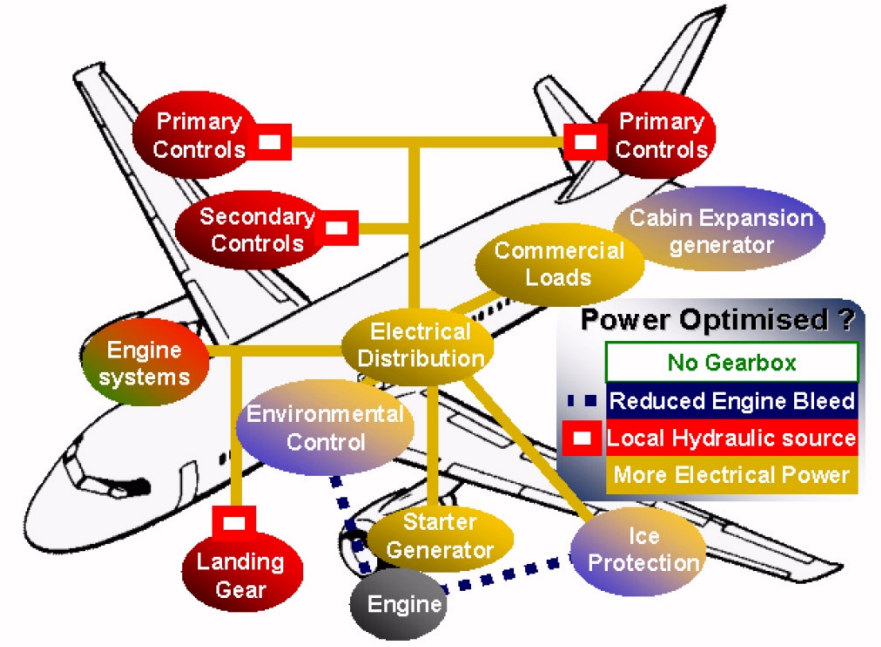

Figure 2.5: Schematic of improved power distribution based mainly on electrical power supply [31].

of new technological solutions. Many research and development programs have been founded in order to reach this goal. The Power Optimised Aircraft project (POA) [30] is the most recent and most integrated project to address the creation of a more efficient aircraft. At the aircraft level, the project should demonstrate a 25% reduction in peak non-propulsive power usage, a 5% reduction in fuel consumption, a reduction in equipment weight and no degradation in production costs, maintainance costs or reliability. This will be achieved by:

- the traditional approach of improving performance of individual systems in terms of acceptable energy consumptions;
- the innovative approach of completely altering the way in which the architecture of aircraft systems is designed.

Let us start considering the second approach. In a conventional architecture, which can be described by the basic schematic shown in Fig. 2.4, fuel is converted into power by the engines. Most of this power is used to move the aircraft. The remainder is directly transmitted to auxiliaries or converted into pneumatic, mechanical, hydraulic and electrical power in order to satisfy non-propulsive power demand. In particular, the ECS receives pneumatic power directly from the engine bleed ports. Up to now the electrical power is the less relevant in the whole energy balance. According to other mobile applications, for example automotive and marine applications, some evidence exists about the fact that a more widespread electrical power distribution would allow us to consider more efficient components and a more flexible management of the energy demand. Both these advantages can yield an increase in the whole efficiency [31]. Let us consider a potential optimized architecture based on this concept, shown in Fig. 2.5. This optimized solution at total aircraft level is certain to define an improvement that any solution at systems level can no longer provide. Obviously some problems may emerge. For example, improving the electri-

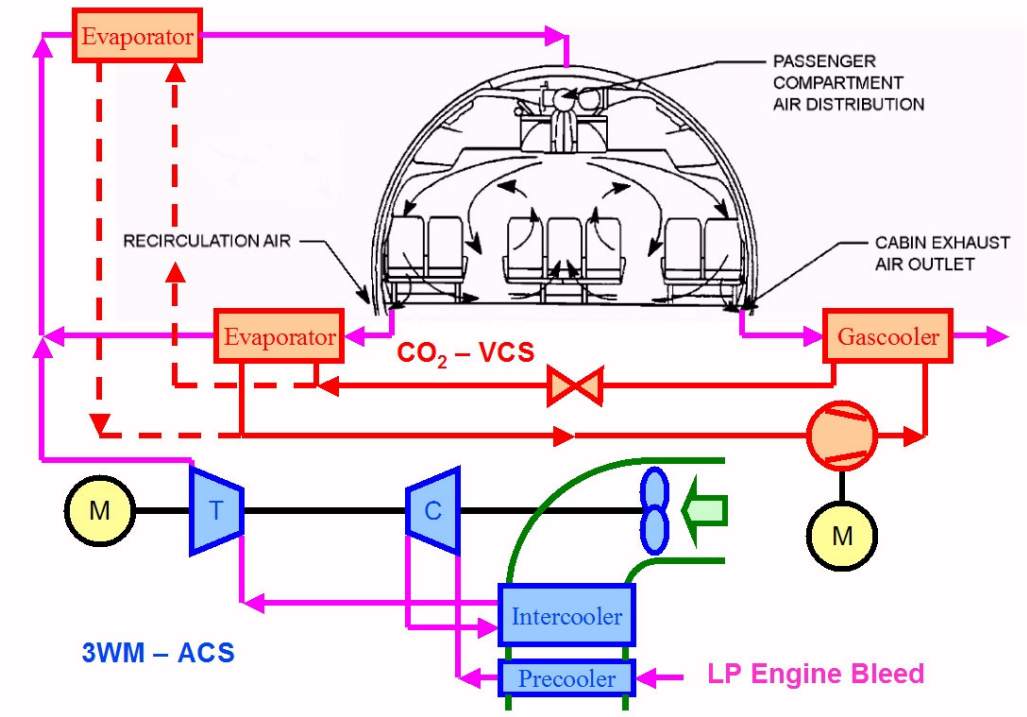

Figure 2.6: Hybrid ECS based on a three-wheel motorized ACS (3WM-ACS) and a carbon dioxide VCS. The motor involved in the air cycle allows us to consider low pressure (LP) engine bleed for the air supply. Two positions of the evaporator in the ECS architecture are considered.

cal power distribution can increase the whole weight of the auxiliaries because the electrical systems tend to be heavier than their conventional equivalents. In order to evaluate the behavior of all systems and to verify the suitability of the adopted architecture on the aircraft level, it is necessary to apply an integrated model of all considered systems. One of the goals of the experimental activity described later on in this work is to validate a mathematical model of the Vapor Cycle System (VCS) in order to yield a reliable simulation tool.

Improving electrical power distribution and increasing the number of the electrical systems can open some opportunities for the ECS too. If a motorized ACS is adopted, the additional mechanical power, which derives from the electrical motor, allows us to

consider a lower pressure engine bleed for the air supply of the Brayton cycle. Since the engine bleed ports may greatly penalize the performance of the engines and this effect is worse for higher pressures, the motorized ACS limits the maximum pressure demand for the engine bleed and produces obvious benefits. This new strategy allows us to remove the high pressure (HP) engine bleed port and keep the low pressure (LP) engine bleed port as it is (the pressure sizing criteria must be applied and the airflow must be defined by the basic fresh flow requirement). In this condition, the motorized ACS is capable of satisfying pressurization, ventilation and cooling/heating during the whole aircraft mission profile except descent. In this phase, normally the engine bleed system switches on HP and the new strategy requires boosting of the motorized ACS to compensate for the lack of the HP engine bleed port.

Nevertheless, something better can be done gaining the efficiency of a Vapor Compression System (VCS), i.e. a system based on a proper closed refrigerant circuit which realizes an Evans-Perkins cycle. In this way, during the whole aircraft mission profile except descent, the ACS is capable to satisfy pressurization and ventilation and the VCS (configured eventually as heat pump) could support the ACS for cooling/heating. The only penalty is again the required pressurization in descent and the motorized ACM boosting is necessary to compensate the lack of HP engine bleed port. This system could be defined a hybrid ECS because it is composed of two subsystems which realize different thermodynamic reference cycles. Two possible integration strategies between subsystems are reported in Fig. 2.6. The refrigerant cooler can be conveniently installed at the cabin exhaust air outlet. Even though the comfort temperature inside the cabin does not ensure the lowest heat sink for the refrigerant cooler (during flight condition the external temperature is usually much lower), this solution allows us to avoid any additional external air inlet and ensure sta-

ble operating conditions. The evaporator can be installed in, at least, two promising locations:

- after the mixing point (AM) between recirculated air taken from the cabin and the refrigerated air as in the 3WM-ACS (see dashed lines in Fig. 2.6);
- before the mixing point (BM) in the recirculation air duct which takes air from the cabin (see continuous lines in Fig. 2.6).

In the first configuration (AM), the evaporator would receive a great air mass flow rate, which is the sum of recirculation and ACS mass flow rate, but it would work with quite low air inlet temperature because of the ACS cooling capacity. The great air mass flow rate tends to reduce the thermal resistance at the evaporator with consequent positive effects in terms of efficiency, while the low air inlet temperature requires low evaporating temperature for the refrigerant and this usually penalizes the compressor. On the other hand, in the second configuration (BM), the situation is reversed because the evaporator would receive a moderate air mass flow rate equal to the fresh flow requirement, but it would work with a higher air inlet temperature equal to the cabin comfort temperature. On the basis of the previous considerations, it is not clear what of these configurations is the best in terms of energy saving. The comparison depends on operating conditions, working fluid, system architecture and adopted components. In order to understand what constraints limit the design process and what configuration yields the best performance, an experimental test rig has been developed. This activity will be discussed later in this work.

The vapor compression refrigerating systems seem promising for airborne application and natural fluids should be considered in order to avoid any future regulation constraint, as it happens now with the air cycle machines. Among the natural fluids

for refrigeration, carbon dioxide seems suitable for this application. Before proceeding with the description of the experimental test rig, a discussion of carbon dioxide characteristics as refrigerant is needed.

2.2 Carbon dioxide as refrigerant

During the ten years that followed the rediscovery of carbon dioxide as refrigerant, there has been a considerable worldwide increase in interest and development activity in this field. Carbon dioxide is very abundant in the environment, waste of many technological processes and used in other widespread technological applications, for example carbonated water. Since it is a natural fluid which has been standing in the biosphere for so many years, its harmlessness is demonstrated with reference with any possible, still unknown, undesired effects. Carbon dioxide is certainly a greenhouse gas, but for its possible use as a refrigerant it should be obtained from industrial waste. In this case, the added greenhouse impact should be considered null, as null is of course its impact on the stratospheric ozone depletion [33].

In the following, only basic theoretical features will be discussed in order to move rapidly to the considered aircraft application. This must not induce to forget that the number of applications for carbon dioxide is increasing. Unfortunately it is difficult to discuss design and practical issues from the general point of view, because the development of components and the way to use properly the specific features of carbon dioxide greatly depends on the specific application.

2.2.1 Historical background

Carbon dioxide has been a natural agent extensively used in the past as a working fluid in vapor compression refrigerating systems, above all in the initial forty years of

the twentieth century [33].

Even though the commercial widespread diffusion of carbon dioxide operating devices had to wait the first years of the twentieth century, the first ideas about how carbon dioxide could be used in refrigeration date back to the nineteenth century. Alexander Twining appears to be the first to propose carbon dioxide as refrigerant in his 1850 British Patent but the first carbon dioxide system was not built until the late 1860s by American Thaddeus S. C. Lowe [20]. Lowe did not develop his idea further. In Europe, Carl Linde built the first carbon dioxide machine in 1881. Franz Windhausen from Brunswick in Germany, in 1886 patented a compressor for a carbon dioxide refrigerating machine. The following year the British Company J. & E. Hall bought a licence to build a carbon dioxide compressor from Windhausen himself. The same company built the first two-stage compressor as well. This can be considered the starting point of the extended use of carbon dioxide as working fluid in mechanical refrigeration.

It is commonly believed that carbon dioxide was exclusively used as a refrigeration fluid aboard ships. It is certainly true that, of the three sectors which drove the rapid expansion of mechanical refrigeration at the beginning of the twentieth century, i.e. ice manufacturing, beer brewing and meat transportation from Australia and Latin America to Great Britain, the latter mainly involved the general use of equipments working with carbon dioxide. This was essentially due to safety reasons aboard ships. But there are also several examples of use of carbon dioxide refrigerating machines in different sectors [34]. Examples are cooling of the ammunition warehouse in warships, in breweries, in wine or liquor cellars, in slaughterhouses, in dairy industries, in artificial ice factories and also in all civil application where the safety issue was considered of prominent importance.

As the CFC were introduced in the 1930s and 1940s, these synthetic refrigerants replaced the old working fluids in most applications. Carbon dioxide was also displaced by this transition to CFC. The reasons of this rapid decline lay certainly in the low energy efficiency of these equipments, the drastic reduction in refrigerating power when ambient temperature increases and finally the problems of refrigerant containment at high pressure, which was difficult with the sealing technology available at that time.

With the CFC problem becoming a pressing issue, Norwegian Gustav Lorentzen believed that the carbon dioxide could have a renaissance as viable refrigerant alternative [35, 36]. In an international patent application, he devised a transcritical carbon dioxide cycle system, where the high-pressure side was controlled by a throttling valve. In 1992, Lorentzen and Pettersen published the first experimental results on a prototype carbon dioxide system for automobile air conditioning. The results about efficiency of this prototype were encouraging, in comparison even with devices based on usual synthetic fluids. For this reason, the interest in carbon dioxide as refrigerant increased considerably throughout the 1990s.

In spite of some encouraging results in particular applications and some potential for more compact components, the widespread diffusion of carbon dioxide is essentially a regulation matter. The emergency of environmental issues based on the depletion of the stratospheric ozone and the display of the anthropogenic greenhouse effect obviously leads to consider more severe regulation. However, since any technological revolution implies some effort, the benefit for the environment must be proportional to this effort. Otherwise some doubts emerge that the same effort could be more usefully applied in another context. A clear and objective analysis of the whole environmental effects due to complete turn-over of synthetic fluids with moderate

environmental effects, like HFCs, in favor of natural fluids, like carbon dioxide, is lacking. Some studies, which have been made for specific applications, may be affected by market strategies and this can increase the confusion about this subject.

2.2.2 Properties of carbon dioxide

Before discussing some peculiarities of refrigerating systems which involve carbon dioxide as working fluid, some of its thermodynamic and transport properties will be reported. The aim of this section is to point out the intrinsic features of carbon dioxide which make it different if compared with traditional refrigerants.

- The main difference is the low value of the critical temperature (see Tab. 2.2) 31.1 $\mathcal{C}$, that is around the maximum summer ambient temperature in Countries with temperated climate. As a consequence, in the traditional vapor compression refrigerating cycle, the process of heat rejection to the environment does not usually imply condensation of carbon dioxide, but a dense gas progressive cooling at (ideally) a constant pressure higher than the critical pressure [34]. The transcritical refrigerating cycle will be discussed later on. Concerning the thermodynamic and transport properties, this feature forces to consider states close to the critical point and consequent critical phenomena.

- A further important difference of carbon dioxide transcritical cycles is given by the much higher pressure levels at equivalent working conditions as far as temperatures of the external source and sink are concerned. Also in this case, the critical pressure (see Tab. 2.2) 73.8 *bar* can help to estimate the pressure levels because usual vapor compression systems based on carbon dioxide work close to and even partially above the critical pressure. As previously outlined even though the carbon dioxide high working pressure does not imply a real bursting

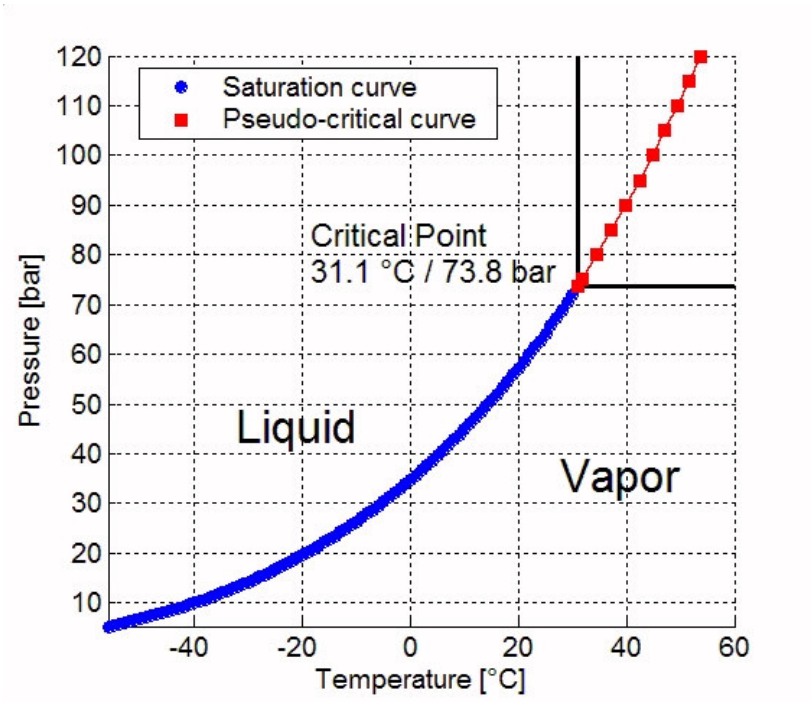

Figure 2.7: Phase diagram for carbon dioxide [96].

danger, it may induce some leakage problems, particularly if elastomeric sealing components are considered.

It is easy to verify that the critical point plays a relevant role in both previous features. The critical point for carbon dioxide is reported in the phase diagram shown in Fig. 2.7. The highest temperature at which condensation/evaporation occurs is known as the critical temperature T_c. Formally, it is possible to define other thermodynamic properties of the critical point. However both theoretical and experimental evidences exist which indicate that the idea of a definite critical point, with unambiguous critical temperature T_c, pressure p_c and volume v_c is probably only an approximation. Actually there appears to be a *critical region* [37]. In order to show how the thermodynamic and transport properties strongly depend on temperature in the critical region, a more detailed discussion is reported. The properties will be

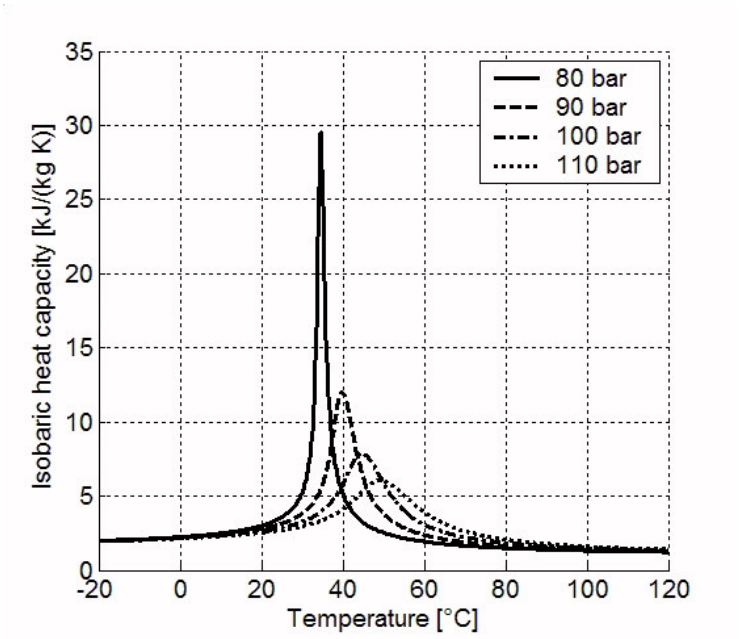

Figure 2.8: Isobaric specific heat capacity for carbon dioxide [96].

divided into three groups: the *thermodynamic properties* (state functions), the *transport properties* (macroscopic effects due to microscopic relaxation phenomena) and *technological properties* (some properties selected from the previous sets which are relevant for this technological application).

1. *Thermodynamic properties*

   In the critical region, the thermodynamic properties have a strong dependence on temperature. In particular the isobaric specific heat capacity at supercritical pressures is characterized by a marked peak for a particular temperature, as shown in Fig. 2.8. For each supercritical pressure, the value of temperature at which the specific heat capacity reaches a peak is called pseudo-critical temperature, T_{pc}. For supercritical pressures, the set of pseudo-critical temperatures defines a pseudo-critical curve, which can be considered as a sort of prolongation of the saturation curve. In Fig. 2.7, both the saturation curve and

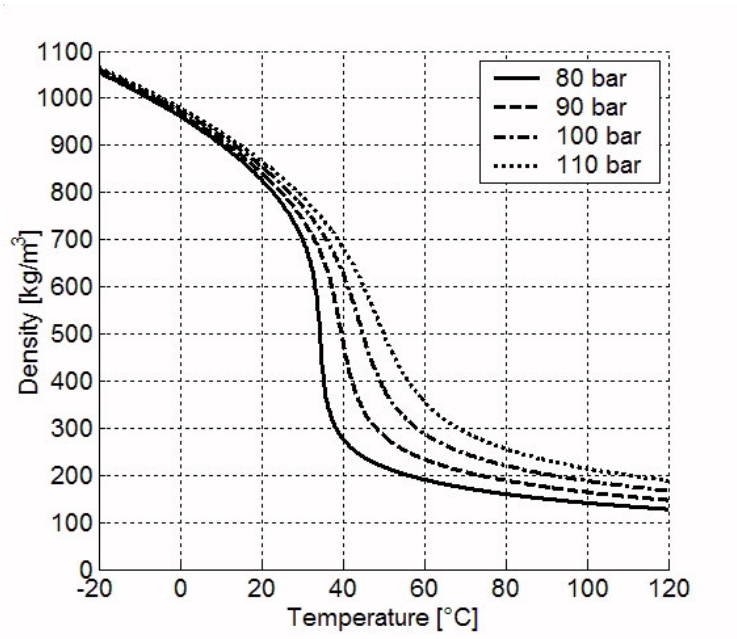

Figure 2.9: Density for carbon dioxide [96].

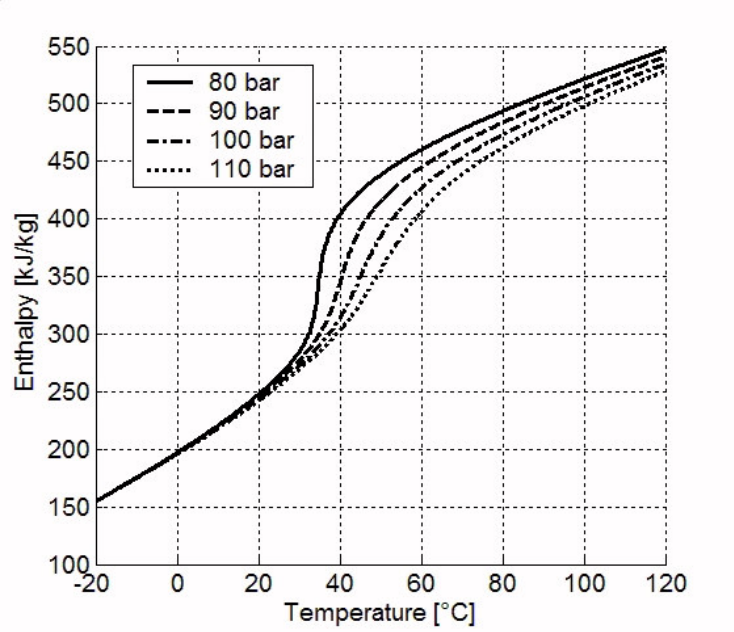

Figure 2.10: Specific enthalpy change for carbon dioxide. The reference enthalpy is equal to 200 kJ/kg for saturated liquid at 0 $℃$, according to what proposed by the International Institute of Refrigeration (IIR) [96].

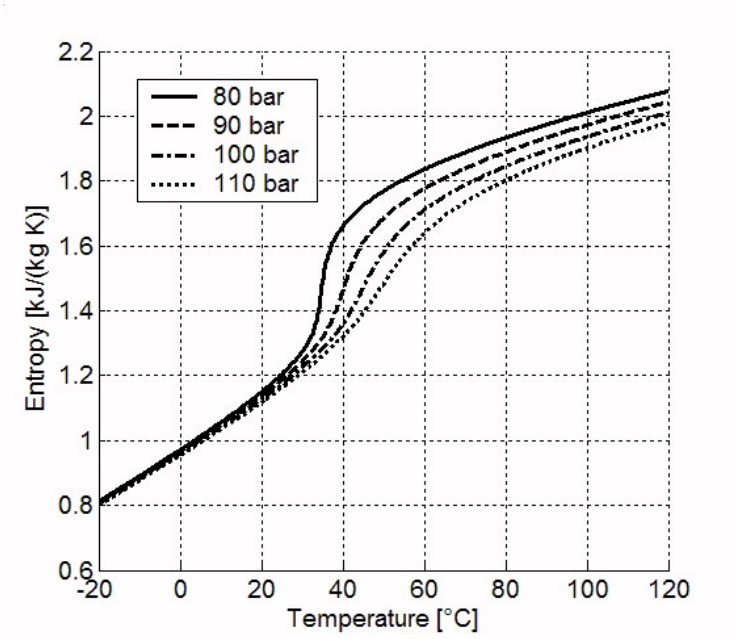

Figure 2.11: Entropy change for carbon dioxide. The reference entropy is equal to 1 $kJ/(kg\,K)$ for saturated liquid at 0 $^{\circ}C$, according to what proposed by the International Institute of Refrigeration (IIR) [96].

pseudo-critical curve are reported. When the bulk temperature decreases below the pseudo-critical temperature for the considered supercritical pressure, the fluid instantaneously changes from a vapor-like state to a liquid-like state [38]. For this reason, the supercritical fluid region ($p_c < p$ and $T_c < T$) can be divided into two sub-regions: the liquid-like region ($p_c < p$ and $T_c < T < T_{pc}$) and the vapor-like region ($p_c < p$ and $T_c < T_{pc} < T$). These concepts will be useful later on for discussing convective heat transfer close to the critical point. It should be noted that the conventional design methods, like for examples the Logarithmic Mean Temperature Difference (LMTD) and the Effectiveness - Number of Transfer Units (ϵ-NTU), based on simplifying assumptions for the isobaric specific heat capacity, cannot be globally applied to design heat exchangers for this application. Since the thermodynamic properties strongly vary with tempera-

ture, the heat exchangers can be numerically described by using discretization meshes of appropriate size.

The density of carbon dioxide changes rapidly with temperature near the critical point too, as shown in Fig. 2.9. At supercritical pressures the density difference between liquid-like states and vapor-like states is much smaller than the difference between liquid phase and vapor phase for pressures below the critical pressure. However, for subcritical pressures, condensation induces a gradual increase in the density, while in this case the increase is very rapid close to the pseudo-critical temperature. Even though the density difference is smaller in this second case, the corresponding density slope with respect to enthalpy $\partial\rho/\partial h$ is much greater. This implies that in turbulent regime high-frequency fluctuations of enthalpy may induce high-frequency fluctuations of density, in addition to common fluctuations of velocity components. For this reason, the turbulence closure models for time-averaged equations must provide some techniques for describing this additional effect. This effect will be discussed in great detail in Chapter 4.

Finally, in Figures 2.10 and 2.11, enthalpy and entropy changes are reported at constant pressure. The enthalpy and entropy decrease with temperature during the cooling process is characterized by more abrupt changes close to the pseudo-critical temperature. In the supercritical region, both enthalpy and entropy strongly depend on pressure .

2. *Transport properties*

The transport properties derive from the microscopic relaxation phenomena and they strongly affect the heat transfer performance. In Figures 2.12 and 2.13, thermal conductivity and dynamic viscosity for carbon dioxide are reported,

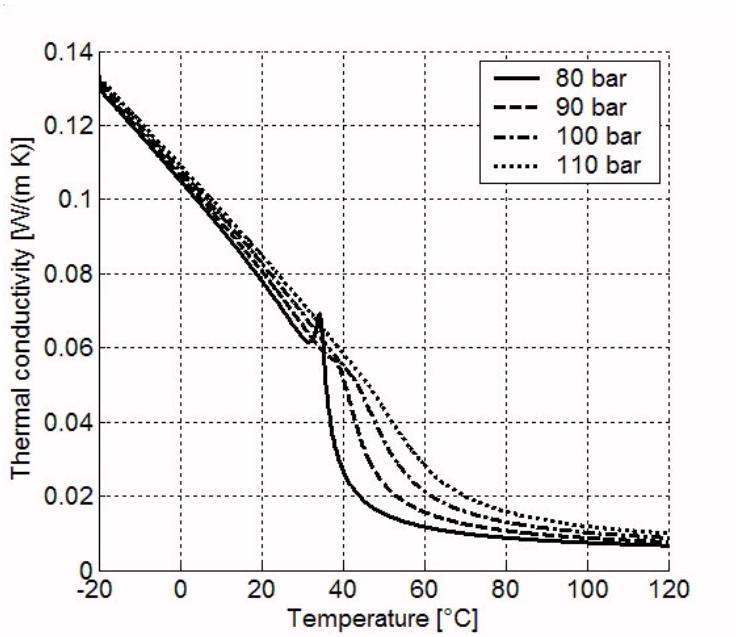

Figure 2.12: Thermal conductivity for carbon dioxide [96].

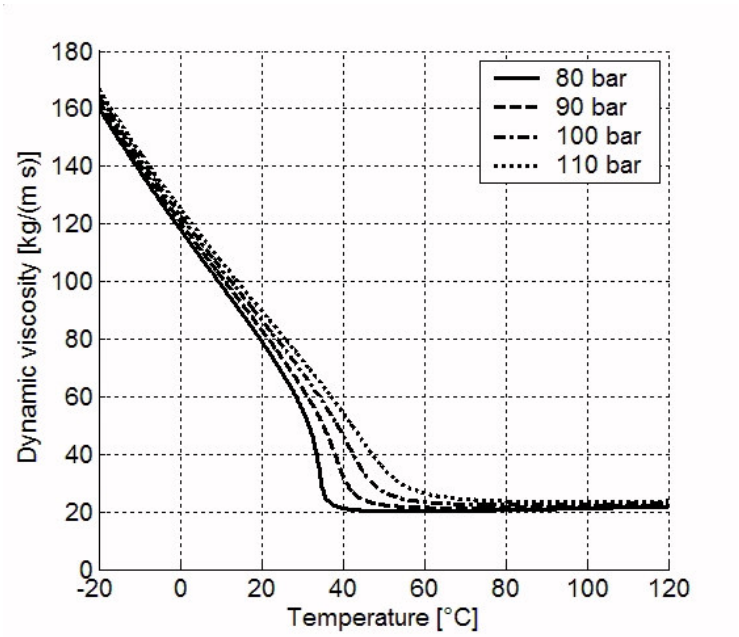

Figure 2.13: Dynamic viscosity for carbon dioxide [96].

respectively. At the pseudo-critical temperature which implies the maximum isobaric specific heat capacity, the thermal conductivity shows a weaker peak too, at least at supercritical pressures closer to the critical point. The dynamic viscosity shows a peculiar behavior too. When the bulk temperature decreases below the pseudo-critical temperature for the considered supercritical pressure, the dynamic viscosity abruptly increases, in order to match the liquid-like behavior. The viscosity and the ratio of liquid to vapor viscosity are important parameters for the fluid flow behavior [20]. Here two features will be pointed out. Firstly, it is easy to verify that the Prandtl number has a maximum at the pseudo-critical temperature associated with the corresponding specific heat capacity, which is the leading property in its definition. This results in a strongly varying local heat transfer coefficient depending on temperature and pressure, which reaches the maximum value for the pseudo-critical temperature. Secondly, as a result of the strong dependence of physical properties on temperature, convective heat transfer at supercritical pressure is generally more complex than common applications. For these reasons, carbon dioxide is characterized by enhanced heat transfer: consequently compact heat exchangers can be realized but some care is required for properly designing these devices.

3. *Technological properties*

The technological properties are some thermodynamic and transport properties which particularly affect the design and the operating conditions of refrigerating machines based on carbon dioxide.

As previously outlined, the first example is the much higher operating pressure at equivalent working conditions, which implies special care for selecting connecting components and for avoiding explosion danger. Fortunately, carbon

dioxide is characterized by a smaller slope of the saturation pressure curve in comparison with conventional refrigerants. For this reason, a smaller temperature change follows a given pressure change and this can reduce the undesired temperature glide due to pressure drops in the two-phase region. For this reason, higher pressure drops are allowed because the relative pressure drops may be modest and the effects in terms of temperature glide may be even more negligible.

As a consequence of high working pressures, the liquid density is much higher than that of conventional refrigerants. The higher vapor density gives the high volumetric refrigeration capacity, which is defined as product of vapor density and latent heat of evaporation. The volumetric refrigeration capacity is 3-10 times larger than other refrigerants and this allows us to design more compact evaporators in order to obtain the same cooling capacity.

Finally, the last technological property considered here is the surface tension. Surface tension affects the growth of vapor bubbles by determining superheat required for nucleation and consequently affects the evaporation heat transfer. Carbon dioxide presents a smaller surface tension than those of other refrigerants.

The previous properties will be useful for characterizing the heat transfer performance of carbon dioxide during the cooling process and consequently the most important features of transcritical thermodynamic cycles.

2.2.3 Transcritical refrigerating cycle

A thermodynamic cycle can be defined transcritical when it involves pressure levels below the critical pressure (subcritical pressures) and above the critical pressure

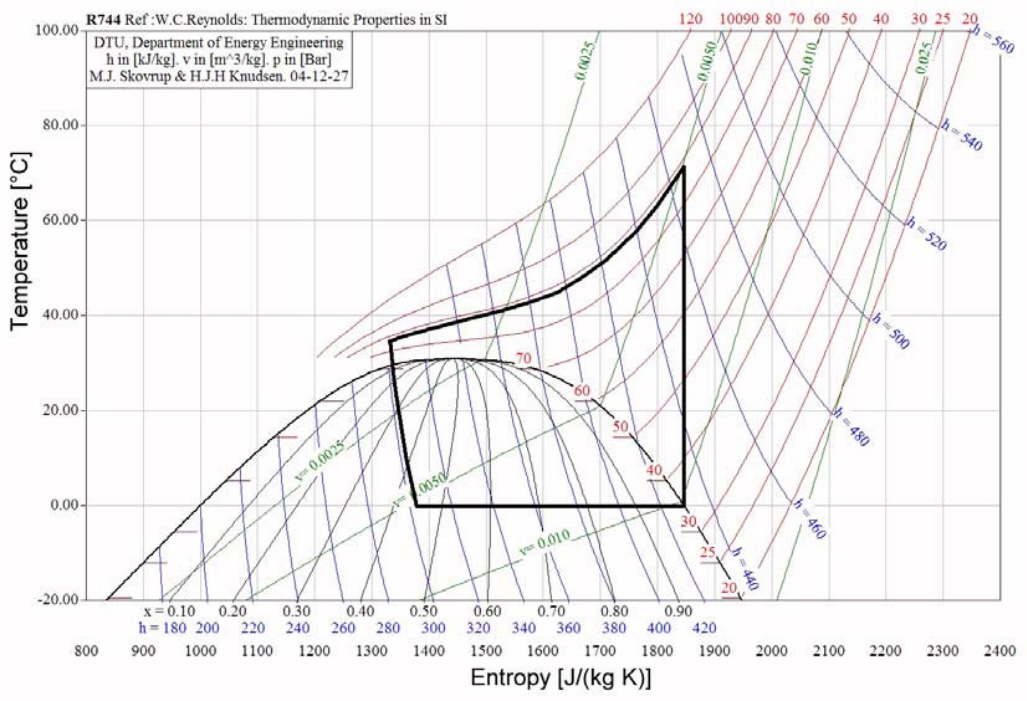

Figure 2.14: Transcritical cycle in the carbon dioxide temperature-entropy diagram.

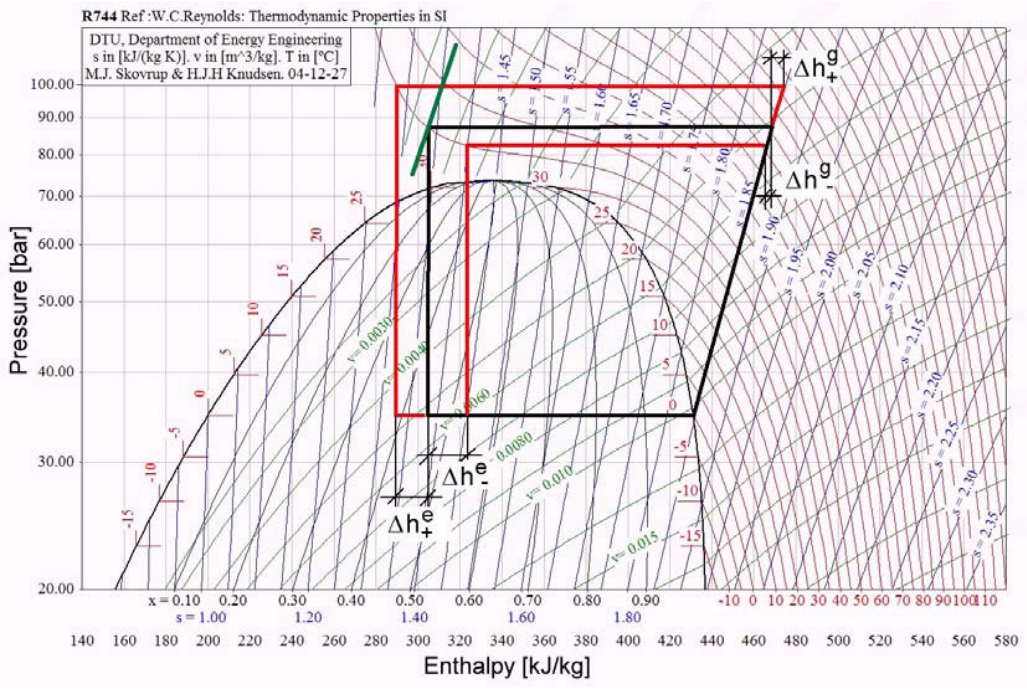

Figure 2.15: Transcritical cycle in the carbon dioxide pressure-enthalpy diagram.

(supercritical pressures). A typical example of a transcritical cycle for carbon dioxide in the temperature-entropy diagram is reported in Fig. 2.14. Obviously, it is possible to design both direct and inverse transcritical cycles. In the following, only single-stage traditional vapor compression refrigerating cycles will be discussed. Since the critical temperature of carbon dioxide is quite low, during the process of heat rejection to the environment it is hard to realize a condensation of the working fluid. For this reason, a dense gas progressive cooling at (ideally) a constant supercritical pressure is considered and the cycle becomes transcritical.

Two are the most important features of the transcritical thermodynamic cycles based on carbon dioxide as working fluid.

- The coefficient of performance (COP) of the transcritical cycle is not a monotonic function of the supercritical discharge pressure which characterizes the dense gas cooling process. In particular, an optimal value of the supercritical pressure, which is function of the considered operating conditions (evaporation temperature, heat sink temperature, superheat of the compressor suction line, isoentropic compression efficiency,...), exists and some devices should be designed to work as close as possible to this favorable condition.

- The heat sink temperature and the consequent gascooler outlet temperature strongly affect the cooling capacity of the transcritical cycle. Since the outlet conditions of the gascooler are usually very close to the critical point, very small temperature changes are enough to produce strong changes of the gascooler outlet enthalpy, which can be identified with the evaporator inlet enthalpy. For this reason, simple transcritical cycles may be very sensitive to environmental conditions and they should be designed in order to access a cooling heat sink with a temperature as constant as possible.

The first feature can be understood by considering the pressure-enthalpy diagram, reported in Fig. 2.15. The shape of the constant-temperature curves explains why an optimum gascooler pressure exists. In fact, at supercritical pressures closer to the critical point, small changes in the discharge pressure induce strong changes in the gascooler outlet enthalpy and this means that in optimal conditions modest additional work of compression can easily widen the evaporation process in terms of specific enthalpy, i.e. it can easily increase the difference between outlet and inlet specific enthalpy of the evaporator. However for a fixed gascooler outlet temperature, an increase in the discharge supercritical pressure does not increase the COP, when the added capacity no longer fully compensates for the additional work of compression. In Fig. 2.15, three transcritical cycles are reported but only the cycle characterized by the intermediate discharge pressure has the best COP.

Moving from the cycle characterized by the intermediate gascooler pressure to that characterized by the lower pressure both the refrigerating effect and the compression work decrease (by Δh^e_- and Δh^c_- respectively). On the other hand, moving from the cycle characterized by the intermediate gascooler pressure to that characterized by the higher pressure both the refrigerating effect and the compression work increase (by Δh^e_+ and Δh^c_+ respectively). In both cases, it depends on the relative changes of the refrigerating effect and the compression work whether the COP decreases or increases. For an ideal simple transcritical cycle, such as those reported in Fig. 2.15, the value of the optimum pressure of the gas cooler can be estimated, as a function of the evaporation temperature and the gascooler outlet temperature [34]. In Fig. 2.15, the optimal discharge pressure for an evaporating temperature of 0 $℃$ is reported as a function of the gascooler outlet temperature by means of an inclined segment. A gascooler pressure below the optimum value can sometimes drastically penalize the

cycle efficiency. The trend of the cycle COP as a function of the gascooler pressure for discharge pressures greater than the optimal one is rather flat. Therefore a slight overpressure in the gascooler with respect to the optimum, does not penalize too much the cycle efficiency.

The second feature which characterizes the transcritical thermodynamic cycles based on carbon dioxide is easier to understand and it is a direct consequence of the thermophysical properties close to the critical point. If the gascooler outlet temperature is close to the pseudo-critical temperature for the considered supercritical pressure, then the isobaric specific heat capacity reaches its maximum and for this reason, small changes in the outlet temperature yield strong changes in the outlet enthalpy. From the thermodynamic point of view, the gascooler outlet enthalpy can be identified with the evaporator inlet enthalpy. Any change to the minimum enthalpy of the cycle will affect directly the cooling capacity and consequently the COP because the compression process can be reasonably considered independent of the gascooler outlet conditions. Let us consider an example: at supercritical pressure of 90 bar, a temperature change of 5 $\mathcal{C}$ close to pseudo-critical temperature yields a enthalpy change of 40 kJ/kg, which is a third of the specific cooling capacity of the optimized cycle reported in Fig. 2.15. In order to properly take into account this phenomenon, an approach temperature difference (ATD) can be introduced. This is the difference between the gascooler outlet temperature and the inlet temperature of the cooling fluid which realizes the heat sink for the refrigerating cycle. Fortunately, heat exchanger design calculations and practical experience show that it is possible to obtain an ATD of a few degrees, even in air-cooled heat exchangers. For this reason, even though this feature is of primary importance, it can be controlled by properly selecting the heat cooling sink and checking that its characteristic temperature is

weakly variable.

There are several ways for modifying the basic single-stage transcritical cycle, both from the thermodynamic and technological point of view, in order to improve the efficiency and/or the cooling capacity for a given system and component size. Exploring and applying these opportunities may seem an obvious trend but it is not what the refrigeration industry usually did during the last fifty years. In particular, two issues worked as conservative factors against any hardware improvement in this field. Firstly, the chemical industry put on the market synthetic fluids designed in order to match the needs of the refrigeration technology. In this way, the research activity focused on searching for and designing the best fluid for any given application. Secondly, low energy prices over most of the twentieth century did not justify investments in research activity aiming to reduce the energy consumption. Both the previous reasons induced to consider the simplest vapor compression cycle in order to reduce the number of components. Nowadays, both these conservative factors lost importance. Today's research is focusing on ways to modify the standard vapor compression cycle by means of multistage compression, intercooling, internal heat exchangers and expanders for work recovery [20]. Rather than searching for a fluid suitable for a defined refrigerating cycle, the current trend is to adapt the cycle to the favorable characteristics of the (hopefully natural) working fluid. In principle, a great number of modifications to the simple transcritical cycle are possible. A complete discussion about all of them is beyond the scope of the present work because essentially they depend on the considered application. Some literature papers can be considered a good starting point in this direction [20, 34, 35].

For airborne systems, it is important to consider a very simple architecture in order to satisfy rigorous constraints about weight reduction and to guarantee the highest

reliability standards. For this reason in the design of the experimental test rig, a very simple architecture has been considered. Some cycle modifications (increasing of heat transfer surfaces for heat rejection and internal heat exchanger) have been considered every time that experimental evidences seemed to require them as the only ways to satisfy the desired goals. This allowed us to limit the number of cycle modifications to minimum value.

2.3 Design and construction of the experimental test rig

An experimental test rig has been designed and built in order to evaluate the performance of a carbon dioxide refrigerating machine based on a transcritical cycle. The test rig reproduces as close as possible the operating conditions of the vapor compression subsystem involved in the hybrid ECS, which is currently under investigation for substituting conventional air-based ECS in commercial aircrafts.

The main goals of this activity are:

1. to produce a coherent set of measurements which will be used to calibrate a simplified mathematical model needed to characterize the vapor compression subsystem;

2. to supply some experimental evidences which allow us to select the most suitable integration strategy between the vapor cycle and the air cycle subsystem, needed to define the whole hybrid ECS (the two most promising strategies are reported in Fig. 2.6).

The most promising aircraft architecture can be selected by running numerical simulations at aircraft level in order to prove the effective improvements due to al-

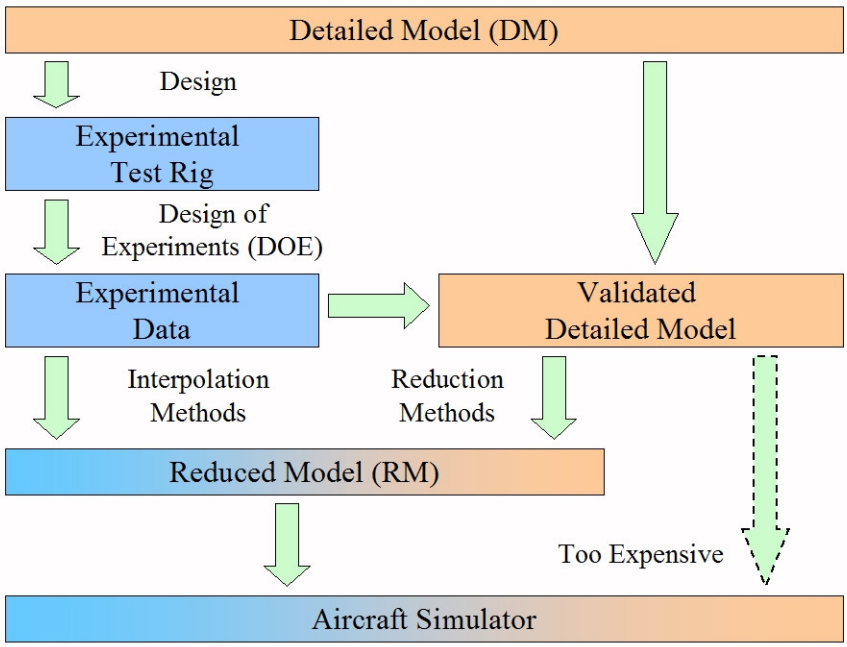

Figure 2.16: A schematic view of the integration between experimental and simulation activity.

ternative solutions and finally to take any action useful to address the creation of a more efficient aircraft. These models include steady-state system models for simulation of long-term behavior, such as power consumption during full flight missions. The steady-state behavior of a considered system may typically consist of parametric analytical functions and/or may be based on existing data sets. These data sets may arise from complex system simulations (e.g. computationally expensive CFD simulations of the cabin airflow in the case of the hybrid ECS model) or experiments, which represent the underlying system behavior. It may be impracticable to fully evaluate the underlying behavior of these systems, in particular if validation or optimization of the integrated system on the aircraft level is considered. In such cases, approximate representations of the behavior of these systems can provide good possibilities for efficient evaluation at low computational cost and with adequate accuracy [32].

Between detailed system simulation and interpolation of experimental data, a third way is possible and it will be here considered for developing the mathematical model of the VCS. In fact, detailed models may be useful during the design process of the experimental test rig, but they require a long computational time which is unacceptable at aircraft level. In theses cases, model reduction methods provide interesting answers, as they allow us to replace a large size model, also called Detailed Model (DM), whose order N corresponds to the number of discretization nodes, by a small size model or Reduced Model (RM) whose order is $n \ll N$. RMs are made up of small systems of equations and they simulate the system thermal behavior for the whole domain or a part of it with limited loss of accuracy and very short computing time. The previous concepts are quite general and they may be applied to the modeling of a single phenomenon [39], a single component or a complex network made of many components. A schematic view of the integration between experimental and simulation activity is reported in Fig. 2.16.

The essential starting point of any reduced model is a reliable detailed model, which produces numerical results close to experimental data according to a given tolerance. Since the validation process could involve infinite experimental configurations, a meaningful design of experiments (DOE) is needed. The selected experiments should be as close as possible to the actual operating conditions of the installed VCS. Unfortunately, a full capacity test rig would be too expensive at this stage because of the lack of existing components for aircraft application. For this reason, smaller components, derived from automotive application, were considered in this work and a proper scaling strategy was considered too.

The steady-state cooling load for a particular aircraft model is determinated by a heat transfer study of several elements (convection at outer aircraft skin, radiation

from external environment, solar radiation through glasses, conduction through aircraft structure, convection at interior aircraft skin,...). These calculations allow us to estimate the refrigerating thermal power needed by the particular aircraft model. Usually, this cooling request is split between two identical ECSs in order to guarantee at least half of the cooling capacity, in case of single system failure. In the present application, this ideal process is more complicate by the fact that the cooling capacity must be further split between the VCS and the ACS which make the ECS. The most suitable splitting ratio is one of the goals of the optimization. A first guess is reported in Tab. 2.3, where only one of the two identical systems has been considered. The sizing criteria for the air conditioning system is usually defined by conditions at ground operation on a hot, humid day with the aircraft fully loaded and doors closed [28]. A cabin temperature of about 25 $^{\circ}C$ is usually specified for these hot-day ground-design conditions. During flight, the system should maintain a cabin temperature of 24 $^{\circ}C$ with a full passenger load and, moreover, the requested cooling capacity is usually smaller than that required by ground conditions because the external environmental temperature is lower [28].

The experimental test rig aims to generate one third of the full cooling capacity for both ground and flight conditions. In order to realize similar temperature profiles and to reproduce operating conditions as close as possible to those of the actual machine at aircraft level, the air mass flow rates for both heat exchangers were chosen to be one third of the actual values too. The heat exchanger inlet temperatures were increased (+5 $^{\circ}C$ for the evaporator and +2 $^{\circ}C$ for the gas cooler) in order to take into account local heatings due to fans and auxiliary devices.

The nominal design conditions and the corresponding ranges for the low capacity test rig are reported in Tab. 2.4. It is a good practice to set the nominal condition

Table 2.3: Selected operating conditions of both full capacity VCS and low capacity VCS test rig.

Full Capacity VCS at Aircraft Level		
	Ground	Flight
Cooling Capacity $[kW]$	22.0	16.0
Cabin Comfort Temperature $[^{\circ}C]$	25	24
Gascooler Air Mass Flow Rate $[kg/s]$	0.90	0.90
Gascooler Air Inlet Temperature $[^{\circ}C]$	27	26
Evaporator after mixing point (AM) (see Figure 2.6)		
Evaporator Air Mass Flow Rate $[kg/s]$	1.40	1.20
Evaporator Air Inlet Temperature $[^{\circ}C]$	20	20
Evaporator before mixing point (BM) (see Figure 2.6)		
Evaporator Air Mass Flow Rate $[kg/s]$	0.80	0.60
Evaporator Air Inlet Temperature $[^{\circ}C]$	30	29

Low Capacity VCS Test Rig (1/3 of Full Capacity)		
	Ground	Flight
Cooling Capacity $[kW]$	7.3	5.3
Gascooler Air Mass Flow Rate $[kg/s]$	0.30	0.30
Gascooler Air Inlet Temperature $[^{\circ}C]$	27	26
Evaporator after mixing point (AM) (see Figure 2.6)		
Evaporator Air Mass Flow Rate $[kg/s]$	0.47	0.40
Evaporator Air Inlet Temperature $[^{\circ}C]$	20	20
Evaporator before mixing point (BM) (see Figure 2.6)		
Evaporator Air Mass Flow Rate $[kg/s]$	0.27	0.20
Evaporator Air Inlet Temperature $[^{\circ}C]$	30	29

Table 2.4: Nominal operating conditions of the low capacity VCS test rig.

	Nominal	Range
Cooling Capacity $[kW]$	6.3	$5.3 \div 7.3$
Gascooler Air Mass Flow Rate $[kg/s]$	0.33	$0.27 \div 0.33$
Gascooler Air Inlet Temperature $[^{\circ}C]$	30	$25 \div 30$
Evaporator Air Mass Flow Rate $[kg/s]$	0.33	$0.20 \div 0.47$
Evaporator Air Inlet Temperature $[^{\circ}C]$	25	$20 \div 30$

for each parameter as mid value of the corresponding range. This practice has been forced for the gascooler. It is precautionary to assume higher temperature for the heat rejection sink because this temperature can strongly penalize the cycle performance. Moreover, the gascooler air mass flow rate should not be smaller than the evaporator one because the former must reject a larger thermal power than that introduced as cooling capacity.

2.3.1 Test rig components and architecture

The current applied research for aircraft air conditioning aims to investigate novel ways of generating and distributing power for non-propulsive auxiliary systems in order to reduce the energy consumption. It does not deal with developing new technologies/components because this would be too expensive in terms of research resources if applied to the whole aircraft and it would not bring an immediately available alternative to the current aircraft architecture. For this reason, the design of the VCS experimental test rig did not start from scratch. Existing prototype components have been taken from automotive application because it shares the same need for lightweight and ultra-compact components. Practically the simplified design of the experimental test rig required to find the best architecture satisfying the desired

performance (see Tab. 2.4) and reducing the number of components to the minimum value.

First of all, the elements which define the test rig can be classified in six categories:

1. *circuit main components*, which realize the transcritical refrigerating circuit (gascooler, evaporator, compressor, throttling valve, internal heat exchanger);
2. *circuit accessories*, which allow the refrigerating machine to work properly (filters, safety valves, external heat exchanger, pipes, connecting components,...);
3. *auxiliary circuit components*, which simulate the thermal load and the heat rejection sink as close as possible to actual operating conditions at aircraft level (air ducts, air fans, local heaters, recirculation piping,...);
4. *mechanical power suppliers*, which provide the mechanical power needed for moving refrigerant/air mass flows and controlling the automatic devices (electrical motors, inverters, pneumatic ports,...);
5. *transducers*, which allow us to perform the measurements and to collect the feedback signals for controlled devices (pressure transducers, temperature transducers, mass flow transducers,...);
6. *softwares*, which allow us to store the measured data, to realize different control strategies and to analyze on-line/off-line the reliability of performed tests (acquisition system, flexible control system, post-processing system,...).

Let us start with the circuit main components. All the heat exchangers of the refrigerating circuit (gascooler, evaporator and internal heat exchanger) derive from automotive application. Figures 2.17 and 2.18 report a picture of a one-slab gascooler and of a one-slab evaporator, respectively. Both gascooler and evaporator are brazed aluminum heat exchangers with flat microchannel tubes and proper manifolds, which

Figure 2.17: Parallel flow brazed aluminum gascooler with flat microchannel tubes, originally developed for automotive application (Obrist Engineering). The microchannel tubes realize a two-pass design. Folded fins without louvers are considered. External sizes for one slab are $615 \,\mathrm{x}\, 353 \,\mathrm{x}\, 13\, mm$ (courtesy of Microtecnica s.r.l.).

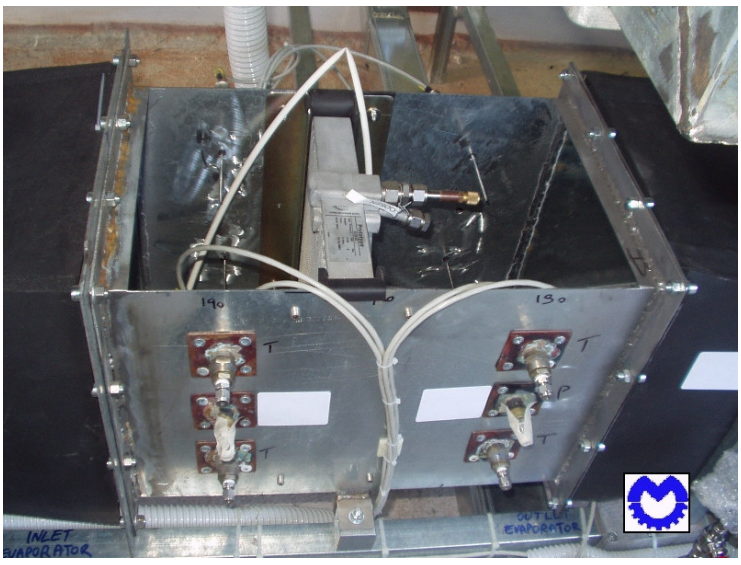

Figure 2.18: Parallel flow brazed aluminum evaporator with flat microchannel tubes, originally developed for automotive application (Obrist Engineering). The microchannel tubes realize a multi-pass design. Folded fins without louvers are considered. External sizes for one slab are $256 \,\mathrm{x}\, 271 \,\mathrm{x}\, 42\, mm$ (courtesy of Microtecnica s.r.l.).

realize multi-pass design in order to improve heat transfer effectiveness. Both have finned air-side surface but the folded fins are smooth, in order to avoid additional air-side pressure drops due to louvers. This technology allows us to have more than 700 m^2 heat transfer surface per 1 m^3 core volume, which is close to the current technological limit for compact heat exchangers. The high working pressure and favorable heat transfer properties of carbon dioxide enable reduced microchannel diameters and small refrigerant-side surface areas [20]. This aspect, with regard to the gascooler, will be discussed later on.

Since the required cooling capacity for the present test rig is greater than that of a conventional air conditioning system for automotive applications, multi-slab configurations for heat exchangers is needed. In order to evaluate the proper architecture for the present application, some numerical simulations were run. A numerical code previously developed was used for this purpose [40] and small changes were introduced (internal heat exchanger) in order to describe the architectures under investigation. The numerical code requires detailed geometrical and topological data of both heat exchangers in order to match real devices and some compressor global performance data. Both the heat exchangers were discretized by means of a proper number of subsystems in order to catch effects due to thermo-physical properties variation with temperature. Finally, the predicted operating conditions and consequent performance were calculated by means of an iterative procedure, aiming to satisfy the thermal balance for both heat exchangers. Heat transfer phenomenological correlations taken from literature were adopted for characterizing heat transfer phenomena and pressure drops. The reliability of the numerical results is guaranteed by an extensive validation process based on experimental data [40]. In the following, this model is regarded as the detailed model, previously discussed about integration between ex-

Table 2.5: Numerical simulations for different system architectures: simple *architecture A* with one-slab gascooler and one-slab evaporator; improved *architecture B* with two-slab gascooler, one-slab evaporator and internal heat exchanger; best *architecture C* with two-slab gascooler, two-slab evaporator and internal heat exchanger.

Architecture	A	B	C
Coefficient of performance $[-]$	0.840	1.434	1.543
Refrigerant mass flow rate $[kg/s]$	0.088	0.056	0.061
Cooling capacity $[kW]$	3.812	6.426	6.970
Mechanical compression power $[kW]$	4.538	4.483	4.517
Rejected thermal power $[kW]$	7.149	10.224	10.526
Wasted compressor thermal power $[kW]$	0.482	0.642	0.643
Wasted discharge line thermal power $[kW]$	0.689	0.371	0.404
Internal thermal power $[kW]$	-	3.289	3.890
Evaporator			
Cooled air mass flow rate $[kg/s]$	0.334	0.334	0.334
Inlet cooled air temperature $[\mathcal{C}]$	25.0	25.0	25.0
Inlet cooled air humidity ratio $[g/kg]$	1.950	1.950	1.950
Outlet cooled air temperature $[\mathcal{C}]$	13.7	6.8	5.0
Outlet cooled air humidity ratio $[g/kg]$	1.947	1.949	1.947
Gascooler			
Cooling air mass flow rate $[kg/s]$	0.326	0.326	0.326
Inlet cooling air temperature $[\mathcal{C}]$	30.0	30.0	30.0
Outlet cooling air temperature $[\mathcal{C}]$	51.3	60.5	61.4

perimental and simulation activity (see Fig. 2.16). The nominal operating conditions for air-side mass flow rates reported in Tab. 2.4 were assumed.

Three architectures were investigated:

- *architecture A*, the simplest and most lightweight architecture made of a one-slab gascooler, a one-slab evaporator, compressor and throttling valve;
- *architecture B*, an improved architecture which doubles the heat rejection surface by assuming a two-slab gascooler and enables to reach lower enthalpy at

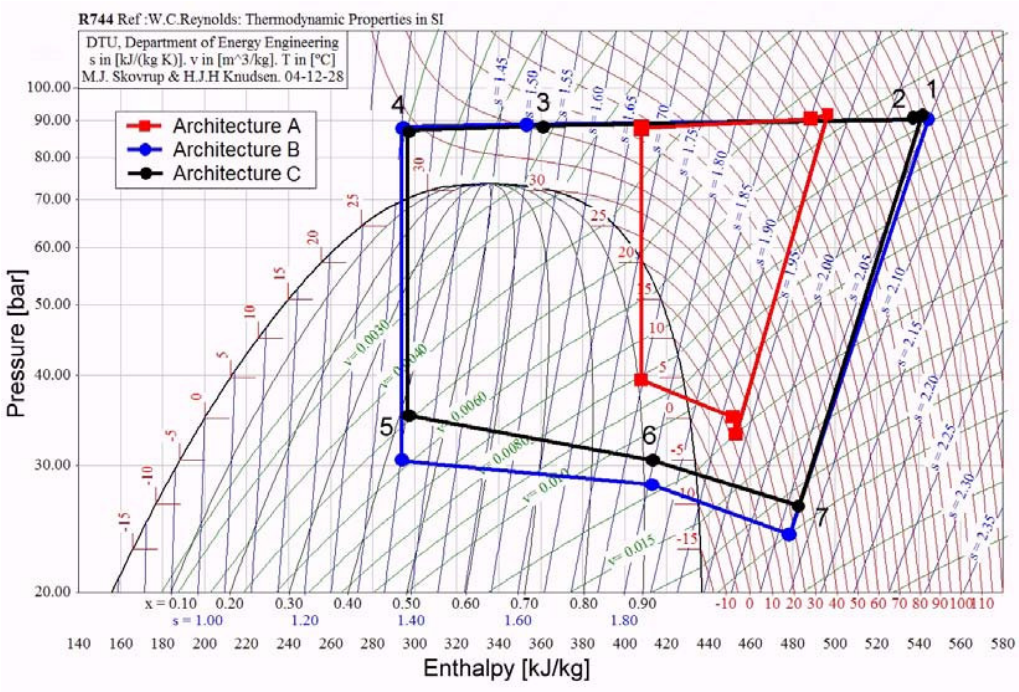

Figure 2.19: Thermodynamic cycles for different system architectures (see Tab. 2.5).

evaporator inlet by adding an internal heat exchanger;

- *architecture C*, a further improved architecture which doubles the heat transfer surface at the evaporator too, by assuming a two-slab evaporator.

The numerical results are reported in Tab. 2.5. Fig. 2.19 shows the simulated cycles in the pressure-enthalpy diagram. The first comment is that the simple *architecture A* does not allow us to satisfy the required cooling capacity ($3.8\ kW < 6.3\ kW$). The test rig must generate only one third of the cooling capacity of the actual VCS at aircraft level. Each VCS at aircraft level provides only half (for safety reasons, two identical systems are expected) of the thermal load assigned to the vapor subsystem by the hybrid ECS. If we roughly assume that the hybrid ECS divides equally the thermal load between air and vapor subsystem, the low capacity VCS of the test rig simulates one twelfth of the actual cooling demand at aircraft level. Two improve-

ments have been considered in order to increase the cooling capacity. Increasing heat transfer surface of the gascooler allows us to reduce the approach temperature and consequently to reduce the gascooler outlet enthalpy, which is equal to the evaporator inlet enthalpy. In the simple *architecture A*, the evaporator must realize a final superheating of the refrigerant in order to avoid liquid suction by the compressor. This penalizes the heat transfer performance of the evaporator because it forces to work in a single-phase region, which is characterized by lower heat transfer coefficients. For this reason, both the improved architectures consider an internal heat exchanger which enables to realize an evaporation process completely in the two-phase region (vapor mass fraction is in the range $0.4 - 0.9$). It is worth to point out that both the previous improvements do not directly involve the evaporator, which is still one-slab. The further *architecture C* considers a two-slab evaporator. In this case, the improvement in terms of cooling capacity is smaller than expected. This proves that the evaporator is a very efficient heat exchanger, which can realize cooling capacities higher that those it was designed for, but the actual limiting constraint for further increasing the cooling capacity is the maximum thermal power which can be rejected by the gascooler. The only benefit of *architecture C* is an increase of the evaporation temperature, which helps to avoid frosting (see Fig. 2.19). The increase in the evaporation temperature slightly modifies the suction conditions for the compressor and this justifies the small discrepancy between the refrigerant mass flow rates of *architecture B* and *C* (see Tab. 2.5). In the experimental test rig, the *architecture C* has been implemented.

Once the heat transfer surfaces have been defined, it is possible to select the proper compressor and the proper rotational speed, which realizes the desired refrigerant mass flow rate. The selected compressor derives from a mobile application too (bus air

Figure 2.20: Single-stage open two-cylinder piston compressor for carbon dioxide with a swept volume of 110 cm^3 and rotational speed range of $500 - 2500$ rpm. It is a pre-series prototype currently under development (Bock $FK - CO_2$). The eight-pole electrical motor has a nominal mechanical power of 11 kW and a nominal rotational speed of 750 rpm at 50 Hz (courtesy of Microtecnica s.r.l.).

conditioning). Figure 2.20 reports a picture of the installed compressor. Essentially it is a single-stage two-cylinder piston compressor for carbon dioxide, which is moved by an external motor. The swept volume is 110 cm^3 and the rotational speed range is $500 - 2500$ rpm. Like the previous heat exchangers, it is a pre-series prototype currently under development too. Taking into account the swept volume, some very easy calculations allow us to estimate the rotational speed required by *architecture* C as included in the range $600 - 800$ rpm (it depends on the actual volumetric efficiency), i.e. close to the lowest allowed speeds. For this reason, the compressor has been coupled with an eight-pole electrical motor with nominal rotational speed of 750 rpm at 50 Hz and nominal mechanical power of 11 kW. In order to investigate different rotational speeds, the electrical motor is supplied with an inverter which enables to tune the electrical frequency in the range $40 - 60$ Hz and, consequently,

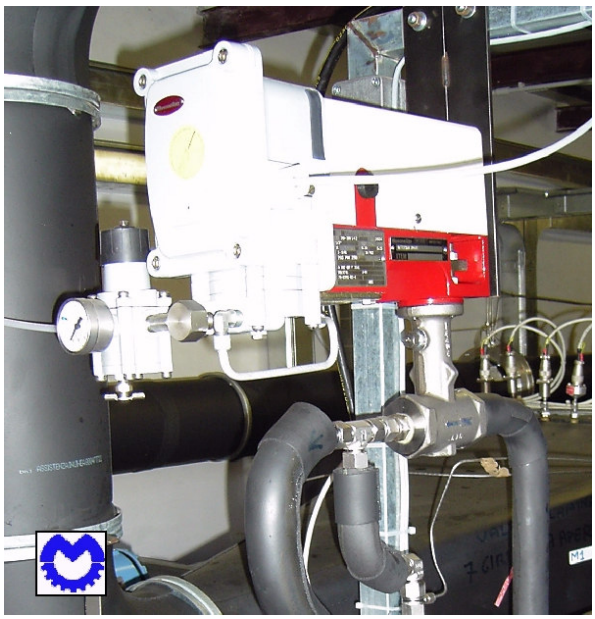

Figure 2.21: Automatic throttling valve with position feedback control (courtesy of Microtecnica s.r.l.).

the rotational speed of the electrical motor in the range $600 - 900\ rpm$.

In transcritical refrigerating cycles, the high-pressure side is no more related to the temperature field inside the heat exchanger designed for heat rejection. For this reason, the high-pressure side becomes a tunable parameter which must be controlled in order to ensure the best COP. There are many different ways of controlling pressure [20]. The easiest way is to use a throttling valve with an adjustable orifice, which temporarily changes the balance between compressor mass flow rate and valve flow rate during transient conditions, in order to vary the high-pressure refrigerant charge. In fact the pressure in the high-pressure side of the circuit is determinated by the relationship between refrigerant charge (mass) inside volume and temperature. Since the total refrigerant charge in the circuit is constant, a refrigerant buffer must be provided so that the high-pressure charge can be varied without flooding or drying up the evaporator. In the present application, an automatic throttling valve with po-

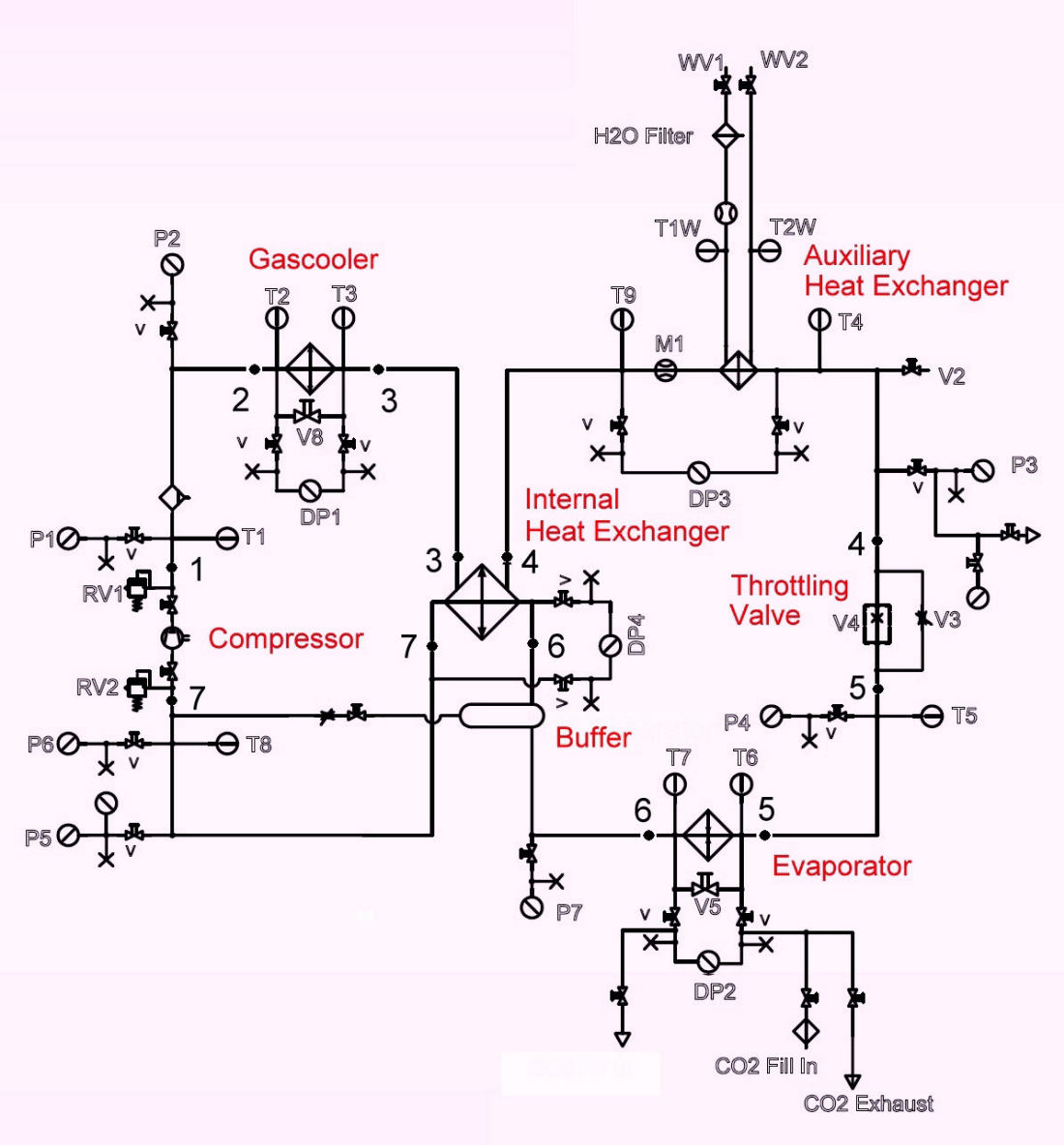

Figure 2.22: Refrigerant-side schematic of the experimental test rig (courtesy of Microtecnica s.r.l.).

sition feedback control and a low-pressure receiver as refrigerant buffer at evaporator outlet have been adopted. A picture of the automatic valve is reported in Fig. 2.21. It allows us to reproduce different control strategies by simply modifying the software settings. In particular, varying the pressure at gascooler outlet (back-pressure working mode) in order to realize the maximum COP according to the inlet temperature of the available heat rejection sink, seems a promising strategy.

The previously discussed main components are collected together in order to realize the refrigerating circuit. Since the operating pressures for transcritical carbon dioxide cycles can be very high (up to 140 *bar*), leakage problems are relevant. For this reason, a double-ogive connecting technology (Swagelok) has been adopted because it should ensure the best sealing. However, the experimental test rig shows a charge reduction due to leakage, which would be unacceptable for a practical prototype working for some months. Fortunately this leakage does not affect the experimental results because the time needed to perform an experimental campaign is usually shorter than the time needed to observe a relevant charge reduction giving a loss of capacity and COP.

A complete refrigerant-side schematic of the experimental test rig is reported in Fig. 2.22. In addition to main components, some circuit accessories, which enable the refrigerating machine to work properly, are needed. The first issue concerns the safety devices. Two safety valves have been adopted in order to avoid explosions at gascooler and evaporator and a third valve allows us to by-pass the automatic throttling valve, if it does not properly work. The compressor was equipped by the manufacturer with two integrated safety valves at suction and discharge line. Another issue is how to introduce the carbon dioxide in the refrigerating circuit. The fill-in and the exhaust connection of carbon dioxide were placed at evaporator inlet. In this way, two

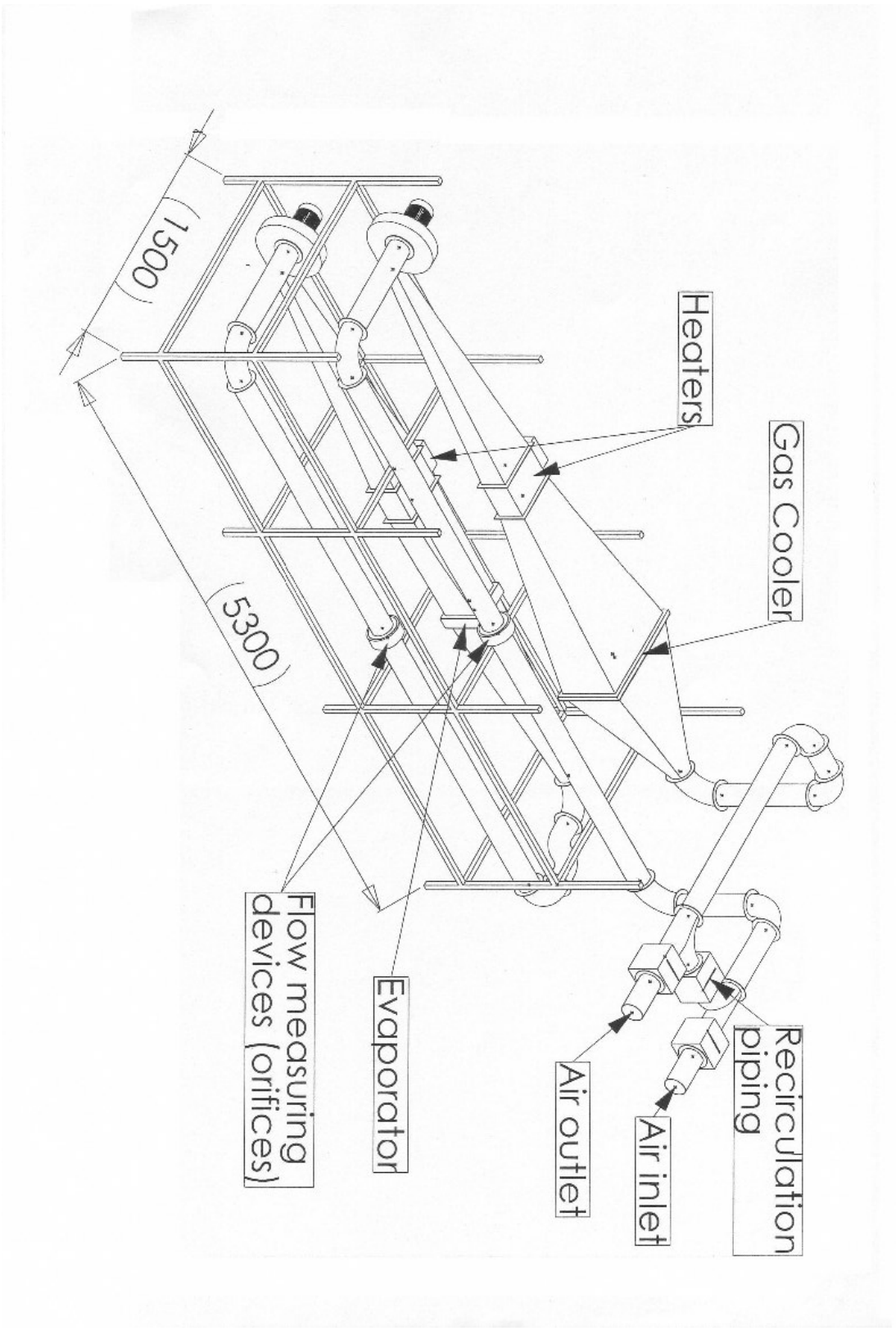

Figure 2.23: Air-side schematic of the experimental test rig (courtesy of Microtecnica s.r.l.).

heat exchangers (evaporator and internal heat exchanger) are interposed between the carbon dioxide storing capacity and the compressor. This should reduce the risk of liquid suction by compressor. Finally an auxiliary heat exchanger (cooling capacity of 100 W at nominal operating conditions) with water as cooling sink has been placed at gascooler outlet. This device allows us to temporarily tune the approach temperature without affecting the performance of the internal heat exchanger.

In addition to the refrigerant circuit, the experimental test rig is made by two air circuits which simulate the thermal load (evaporator air circuit) and the heat rejection sink (gascooler air circuit) as close as possible to actual operating conditions at aircraft level. A schematic of both air circuits is reported in Fig. 2.23. The evaporator is housed in a closed air circuit, while the gascooler is housed in an open air circuit which can take air from the external environment or partially recirculate it in order to reduce the energy consumption. Both the air circuits involve an air fan which generates the desired mass flow rate, a calibrated orifice for measurement purposes and a local heater. The local heater of the evaporator air circuit must compensate the cooling capacity realized by the refrigerating circuit. Since this circuit is practically closed, the air contained inside the circuit is progressively dehumidified and the condensed water is extracted by a proper device. This allows us to suppose that, for steady state conditions, the evaporator air is characterized by very low humidity, independently of external environment. For this reason, the sensible cooling capacity largely dominates over the latent cooling capacity and the latter can be practically neglected for the present application. This peculiarity greatly simplified the design of experiments because a degree of freedom was removed and the time needed to perform an experimental test was shortened. This simplification is acceptable because some evidences suggest that it is more convenient to assign the whole latent cooling

Table 2.6: Installed transducers for VCS test rig in main refrigerating circuit, gas-cooler air circuit (GAC) and evaporator air circuit (EAC).

Transducer Type and Location	Range	Accuracy	N.
Micromotion Flow (Nickel Alloy)	$10/150\ g/s$	$\pm 0.75\%$	1
Micromotion Flow (Stainless Steel)	$10/250\ g/s$	$\pm 0.75\%$	1
Micromotion Transmitter	–	–	2
Temperature Sensor $PT100$	$-50/200\,℃$	$\pm 0.1\%$	45
Refrigerating circuit			9
Environmental air inlet and outlet (GAC)			2
Upstream calibrated orifice (GAC)			1
Upstream local heater (GAC)			1
Upstream of air-side gascooler (PID feedback)			1
Downstream of air-side gascooler			20
Upstream calibrated orifice (EAC)			1
Upstream local heater (EAC)			1
Upstream of air-side evaporator (PID feedback)			4
Downstream of air-side evaporator			4
Relative Pressure Sensor	$0/160\ bar$	$\pm 0.5\%$	6
Refrigerating circuit			6
Pressure Difference Sensor	$0/6\ bar$	$\pm 0.5\%$	2
Astride of refrigerant-side gascooler			1
Astride of refrigerant-side evaporator			1
Pressure Difference Sensor	$0/100\ mbar$	$\pm 2\%$	2
Astride of air-side gascooler			1
Astride of air-side evaporator			1
Pressure Difference Sensor	$0/25\ mbar$	$\pm 2\%$	2
Astride of calibrated orifice (GAC)			1
Astride of calibrated orifice (EAC)			1
Absolute Pressure Sensor	$0/1600\ mbar$	$\pm 0.5\%$	2
Upstream of air-side gascooler			1
Upstream of air-side evaporator			1

capacity to the ACS. In this way, it would be easier to extract the condensed water and to ensure sanitary conditions by avoiding large wet surfaces. Anyway, it is possible to estimate the true cooling capacity including latent thermal power by means of simplified tools (like for example the experimental by-pass factor), which require to know only the sensible thermal power. The local heater of the gascooler air circuit allows us to test severe operating conditions due to an increase in cabin temperature. Both the local heaters are made by electrical resistances and can ensure a maximum thermal power of 10 kW. Both the air fans are moved by two-pole electrical motors with nominal rotational speed of 3000 rpm at 50 Hz and nominal mechanical power of 2.3 kW. Both the electrical motors are supplied by inverters which enable to gradually tune the rotational speed from zero to the maximum value.

The experimental test rig was equipped with some transducers which allowed us to perform the measurements and to collect the feedback signals for the controlled devices. A list of the most important transducers is reported in Tab. 2.6. Essentially the network of transducers has been designed in order to completely characterize the actual thermodynamic cycle and to estimate the air-side thermal powers involved in both air circuits. The last feature enables to check the thermal balance of each heat exchanger and to consequently verify the reliability of the experimental results. The air inlet temperatures for the gascooler and the evaporator in the respective air circuits are controlled by means of two independent PID (proportional-integral-derivative) controllers. The controllers tune the thermal power introduced into air circuits by local heaters in order to force the air inlet temperatures to become equal to the user-defined values.

Finally, the experimental test rig has been provided by a data acquisition system and an on-line post-processing system. The data acquisition system allows us to

Figure 2.24: Vapor Cycle Subsystem test rig (courtesy of Microtecnica s.r.l.).

store the measured quantities on 64 independent channels (currently 61 channels are used) with a frequency of $1 - 2\ Hz$, which is enough to obtain meaningful results with regard to heat transfer phenomena. The post-processing system allows us to check, in every moment during the experimental test, the performances of the actual refrigerating cycle in terms of cooling capacity and COP, the thermal balance of both gascooler and evaporator and the time rate of change of meaningful quantities. The last features are useful to evaluate the effects on cycle performances due to the fill-in process of carbon dioxide and to establish the reached steady state conditions, which conclude the test.

A picture of the whole experimental test rig is reported in Fig. 2.24. In the following, the design of experiments will be discussed and the experimental results will be analyzed.

2.3.2 Design of experiments and analysis of the results

The design of experiments deals with the problem of deciding what pattern of experimental test conditions will best reveal aspects of investigated phenomena and will best allow us to validate the reduced model [41]. To perform a general experimental design, a fixed number of discrete values ("levels") for each of a number of variables ("factors") is selected and then all the possible combinations are experimentally considered. The goal of the experimental design is to characterize how the investigated quantity ("response") depends on considered factors. Obviously the same experimental design can allow us to investigate multiple responses, if they all come from the same phenomenon. If there are l_1 levels for the first variable, l_2 for the second,... and l_k for the k^{th}, the complete arrangement of $l_1 \times l_2 \times \cdots \times l_k$ experimental runs is called an $l_1 \times l_2 \times \cdots \times l_k$ factorial design.

For the present application, there are six meaningful factors: the air mass flow rate at the evaporator inlet G_e; the air mass flow rate at the gascooler inlet G_g; the air temperature at the evaporator inlet T_e; the air temperature at the gascooler inlet T_g; the working pressure at the gascooler outlet p_{bp} and finally the refrigerant mass flow rate G. Possible responses are the cooling capacity Φ_e, the rejected thermal power Φ_g and the thermal coefficient of performance TCOP. The TCOP is defined as:

$$TCOP = \frac{\Phi_e}{\Phi_g + (\Phi_{rh} - \Phi_{rl}) + \Phi_d - \Phi_e} = \frac{\Phi_e}{W_c - \Phi_c}, \tag{2.1}$$

where Φ_{rh} is the high-pressure-side thermal power due to the internal heat exchanger, Φ_{rl} is the low-pressure-side thermal power due to the internal heat exchanger, Φ_d is the thermal power waste of the compressor discharge line, W_c is the mechanical power absorbed by the compressor and Φ_c is the compressor thermal power waste. In the previous definition of TCOP, non-ideal insulation forces to consider additional terms: $\Phi_{rh} - \Phi_{rl} \geq 0$, $\Phi_d \geq 0$ and $\Phi_c \geq 0$. The $TCOP$ differs from the usual coefficient of performance $COP = \Phi_e/W_c$. Taking into account the definition of isoentropic efficiency $\varrho_{is} = W_c^{is}/W_c$, where W_c^{is} is the isoentropic mechanical power needed to perform an ideal compression with constant entropy, the following correlation between TCOP and COP holds:

$$TCOP = \frac{W_c^{is}}{W_c - \Phi_c} \frac{COP}{\varrho_{is}}. \tag{2.2}$$

Since in the experimental tests $W_c - \Phi_c \approx W_c^{is}$, then $TCOP \approx COP/\varrho_{is} \geq COP$. In the design of the experimental test rig, the direct measurement of the mechanical power need has been neglected because the final goal of the present activity is to produce some indications about the best architecture for ECS and to produce a reduced mathematical model, which allows us to characterize the system performance starting from the component performances. For this reason, the available experimental data on compressor performance are enough to calculate the COP starting from the

Table 2.7: Factorial design for the present application. The design of experiments has been defined by air-side operating conditions only. It is possible to group the experimental runs characterized by same operating conditions for each heat exchanger. This yields six classes for the evaporator ($E1-6$), with four runs each, and four classes for the gascooler ($G1-4$), with six runs each.

Run	Air Flow Rate $[kg/s]$		Air Inlet Temperature $[\mathcal{C}]$		Air-side Classes	
	Evap.	Gasc.	Evap.	Gasc.	Evap.	Gasc.
1	0.33	0.33	25	25	E4	G2
2	0.33	0.33	25	30	E4	G1
3	0.33	0.33	30	25	E3	G2
4	0.33	0.33	30	30	E3	G1
5	0.33	0.27	25	25	E4	G4
6	0.33	0.27	25	30	E4	G3
7	0.33	0.27	30	25	E3	G4
8	0.33	0.27	30	30	E3	G3
9	0.27	0.33	25	25	E6	G2
10	0.27	0.33	25	30	E6	G1
11	0.27	0.33	30	25	E5	G2
12	0.27	0.33	30	30	E5	G1
13	0.27	0.27	25	25	E6	G4
14	0.27	0.27	25	30	E6	G3
15	0.27	0.27	30	25	E5	G4
16	0.27	0.27	30	30	E5	G3
17	0.40	0.33	25	25	E2	G2
18	0.40	0.33	25	30	E2	G1
19	0.40	0.33	30	25	E1	G2
20	0.40	0.33	30	30	E1	G1
21	0.40	0.27	25	25	E2	G4
22	0.40	0.27	25	30	E2	G3
23	0.40	0.27	30	25	E1	G4
24	0.40	0.27	30	30	E1	G3

TCOP, measured by this experimental test rig.

The number of factors can be reduced. First of all, the refrigerant pressure at the gascooler outlet should be set equal to the optimal value for the considered approach

Table 2.8: Experimental results for the first set of runs $(1-8)$ defined by the factorial design (see Table 2.7). Pressure, temperature and enthalpy (IIF reference state) are reported for seven meaningful points $(P1-7)$ which define the refrigerating cycle. See Figure 2.19 for adopted labeling of meaningful cornerstones.

P	Run #	1	2	3	4	5	6	7	8
1	p $[\pm 0.7\,bar]$	87.3	92.1	90.5	94.8	89.9	94.2	93.7	97.9
	T $[\pm 0.2\,℃]$	114.1	118.6	118.5	121.7	119.4	122.5	121.7	124.8
	h $[\pm 0.6\,kJ/kg]$	534.6	537.5	538.3	539.8	539.8	541.2	540.5	541.9
2	p $[\pm 0.7\,bar]$	86.1	90.8	89.3	93.5	88.7	92.9	92.3	96.6
	T $[\pm 0.2\,℃]$	108.5	113.1	112.9	116.2	113.8	116.8	116.0	119.1
	h $[\pm 0.6\,kJ/kg]$	528.2	531.0	531.9	533.5	533.4	534.6	533.9	535.2
3	p $[\pm 0.7\,bar]$	83.2	87.8	86.4	90.5	85.8	89.9	89.3	93.5
	T $[\pm 0.1\,℃]$	37.0	40.1	38.3	41.2	38.9	41.9	40.5	43.5
	h $[\pm 0.4\,kJ/kg]$	353.3	359.4	346.4	356.1	359.3	366.3	355.0	362.7
4	p $[\pm 0.7\,bar]$	82.6	87.2	85.8	89.8	85.1	89.2	88.6	92.7
	T $[\pm 0.1\,℃]$	30.8	33.2	32.2	34.9	33.1	35.3	34.5	36.7
	h $[\pm 0.4\,kJ/kg]$	285.9	292.9	289.2	299.4	295.2	302.4	298.5	305.4
5	p $[\pm 0.4\,bar]$	32.8	33.7	34.1	35.4	33.5	34.5	35.1	36.2
	T $[\pm 0.1\,℃]$	-2.2	-1.3	-0.7	0.6	-1.5	-0.4	0.4	1.4
	h $[\pm 0.3\,kJ/kg]$	285.9	292.9	289.2	299.4	295.2	302.4	298.5	305.4
6	p $[\pm 0.4\,bar]$	31.4	32.3	32.8	34.0	32.1	33.0	33.7	34.7
	T $[\pm 0.1\,℃]$	-3.8	-2.8	-2.3	-0.9	-3.0	-2.0	-1.2	-0.1
	h $[\pm 0.3\,kJ/kg]$	407.5	410.0	419.9	421.9	413.6	414.7	422.3	422.7
7	p $[\pm 0.4\,bar]$	27.2	28.1	28.6	29.8	28.0	28.9	29.6	30.6
	T $[\pm 0.1\,℃]$	18.7	21.0	22.6	25.2	22.2	24.1	25.2	27.2
	h $[\pm 0.3\,kJ/kg]$	471.6	473.1	474.2	475.7	474.5	475.5	476.0	477.0

Table 2.9: Experimental results for the second set of runs $(9-16)$ defined by the factorial design (see Table 2.7). Pressure, temperature and enthalpy (IIF reference state) are reported for seven meaningful points $(P1-7)$ which define the refrigerating cycle. See Figure 2.19 for adopted labeling of meaningful cornerstones.

P	Run #	9	10	11	12	13	14	15	16
1	p $[\pm 0.7\,bar]$	91.3	97.3	96.5	101.9	96.4	101.3	101.1	106.9
	T $[\pm 0.2\,℃]$	107.6	111.8	110.2	115.1	110.9	116.1	115.7	120.3
	h $[\pm 0.6\,kJ/kg]$	523.2	524.9	523.1	526.4	524.3	528.1	527.6	530.3
2	p $[\pm 0.7\,bar]$	89.9	95.8	95.0	100.4	95.0	99.8	99.6	105.3
	T $[\pm 0.2\,℃]$	103.3	107.5	106.0	110.9	106.9	111.7	111.3	115.9
	h $[\pm 0.6\,kJ/kg]$	518.4	520.0	518.3	521.4	519.7	523.0	522.6	525.2
3	p $[\pm 0.7\,bar]$	86.4	92.3	91.3	96.7	91.3	96.2	95.8	101.5
	T $[\pm 0.1\,℃]$	39.2	42.8	41.2	44.5	42.2	45.4	44.0	47.5
	h $[\pm 0.4\,kJ/kg]$	358.3	362.6	351.6	357.2	361.4	367.2	357.0	362.3
4	p $[\pm 0.7\,bar]$	85.6	91.4	90.4	95.7	90.4	95.3	95.0	100.6
	T $[\pm 0.1\,℃]$	26.5	29.0	27.7	29.9	28.3	30.7	29.8	32.2
	h $[\pm 0.4\,kJ/kg]$	266.6	272.3	268.4	273.4	270.5	276.2	273.4	279.6
5	p $[\pm 0.4\,bar]$	31.6	32.6	33.3	34.3	32.5	33.3	34.0	35.0
	T $[\pm 0.1\,℃]$	-3.7	-2.5	-1.6	-0.6	-2.6	-1.7	-0.9	0.2
	h $[\pm 0.3\,kJ/kg]$	266.6	272.3	268.4	273.4	270.5	276.2	273.4	279.6
6	p $[\pm 0.4\,bar]$	30.0	31.0	31.7	32.6	30.9	31.6	32.3	33.3
	T $[\pm 0.1\,℃]$	-5.5	-4.3	-3.5	-2.5	-4.5	-3.6	-2.8	-1.7
	h $[\pm 0.3\,kJ/kg]$	363.4	365.7	372.7	374.0	363.8	366.9	375.0	377.6
7	p $[\pm 0.4\,bar]$	24.9	25.9	26.4	27.3	25.8	26.5	27.1	28.0
	T $[\pm 0.1\,℃]$	-1.5	0.6	1.6	4.2	-0.4	2.9	4.5	7.1
	h $[\pm 0.3\,kJ/kg]$	450.5	451.4	451.7	453.5	450.2	453.4	454.4	456.2

Table 2.10: Experimental results for the third set of runs $(17-24)$ defined by the factorial design (see Table 2.7). Pressure, temperature and enthalpy (IIF reference state) are reported for seven meaningful points $(P1-7)$ which define the refrigerating cycle. See Figure 2.19 for adopted labeling of meaningful cornerstones.

P	Run #	17	18	19	20	21	22	23	24
1	p $[\pm 0.7\,bar]$	88.5	92.1	91.5	95.9	91.4	95.1	95.1	99.2
	T $[\pm 0.2\,℃]$	123.1	127.3	126.4	130.4	128.2	131.1	130.1	133.3
	h $[\pm 0.6\,kJ/kg]$	545.6	548.6	547.9	550.4	550.2	551.8	550.5	552.3
2	p $[\pm 0.7\,bar]$	87.4	91.0	90.4	94.7	90.2	93.8	93.8	97.9
	T $[\pm 0.2\,℃]$	116.7	120.8	120.0	123.9	121.6	124.6	123.7	126.9
	h $[\pm 0.6\,kJ/kg]$	538.0	541.0	540.4	542.7	542.6	544.1	543.0	544.7
3	p $[\pm 0.7\,bar]$	84.9	88.4	87.8	92.1	87.6	91.1	91.1	95.1
	T $[\pm 0.1\,℃]$	37.7	40.1	38.6	41.5	39.6	42.2	41.0	43.8
	h $[\pm 0.4\,kJ/kg]$	349.0	355.8	340.9	349.8	354.6	362.3	349.9	358.1
4	p $[\pm 0.7\,bar]$	84.3	87.8	87.2	91.4	87.0	90.5	90.4	94.4
	T $[\pm 0.1\,℃]$	34.7	36.9	36.0	38.5	36.6	38.7	38.1	40.5
	h $[\pm 0.4\,kJ/kg]$	309.5	319.2	312.7	322.6	320.5	327.7	322.2	330.1
5	p $[\pm 0.4\,bar]$	33.3	34.2	34.6	35.6	34.0	35.0	35.6	36.6
	T $[\pm 0.1\,℃]$	-1.7	-0.7	-0.2	0.9	-0.9	0.2	0.9	1.9
	h $[\pm 0.3\,kJ/kg]$	309.5	319.2	312.7	322.6	320.5	327.7	322.2	330.1
6	p $[\pm 0.4\,bar]$	31.4	32.2	32.6	33.5	32.0	32.9	33.5	34.4
	T $[\pm 0.1\,℃]$	-3.9	-3.0	-2.5	-1.5	-3.1	-2.1	-1.5	-0.5
	h $[\pm 0.3\,kJ/kg]$	444.9	449.1	456.9	459.5	451.7	452.4	458.6	459.9
7	p $[\pm 0.4\,bar]$	27.3	28.1	28.5	29.4	28.1	29.0	29.5	30.4
	T $[\pm 0.1\,℃]$	28.3	30.5	30.8	33.2	30.6	32.6	32.9	35.1
	h $[\pm 0.3\,kJ/kg]$	482.4	483.9	483.8	485.3	484.0	485.2	485.0	486.5

temperature in order to realize the maximum COP. Moreover, the refrigerant mass flow rate is mainly a result of the compressor rotational speed because suction cannot change too much for the considered operating conditions and the same holds for the volumetric efficiency according to the results of specific tests on the compressor alone. For these reasons, both previous quantities will be investigated numerically by means of the reduced mathematical model. Only the air-side quantities will be considered for the experimental design. The minimum number of levels (2) will be considered for all factors, with the exception of the air flow rate at the evaporator inlet where 3 levels will be considered because the range of this parameter is wider (see Tab. 2.4). The previous assumptions define a $3 \times 2 \times 2 \times 2$ factorial design, which requires 24 runs. The experimental design is reported in Tab. 2.7. For a given design, it is possible to extract an experimental sub-design by considering a proper sub-set of factors. For example, let us suppose to fix all the factors related to the evaporator, i.e. G_e and T_e. This defines a 2×2 factorial sub-design with 4 runs for the residual factors, i.e. G_g and T_g. Since the number of runs of the whole experimental design is greater than that of the sub-design ($24 > 4$ in the reported example), it is possible to use these additional data for statistically estimating the effects due to the factors kept constant for each sub-design. This issue will be discussed later on when dealing with the reduced model. The sub-designs for both evaporator and gascooler are reported in Tab. 2.7, too.

In order to characterize the thermodynamic cycle, let us consider the following components only: discharge line (d subscript), gascooler (g subscript), high-pressure-side internal heat exchanger (rh subscript), throttling valve (v subscript), evaporator (e subscript), low-pressure-side internal heat exchanger (rl subscript) and compressor (c subscript). Consequently let us define the following cornerstone labels (see

Table 2.11: Comparison between air-side (AS) and refrigerant-side (RS) measurements. The thermal balance for both the heat exchangers is verified by means of the relative percentage error (R), defined as $R = (AS - RS)/RS \times 100$. The air-side measurements have not been performed for the third set of runs $(17 - 24)$.

	Thermal Power							
	Gascooler $[kW]$			Evaporator $[kW]$			Internal	TCOP
	Air-Side	Refr.-Side	R	Air-Side	Refr.-Side	R	$[kW]$	$[-]$
1	10.88	10.45	3.97	8.31	7.27	12.50	3.83	1.93
2	10.69	10.46	2.15	8.11	7.13	12.00	3.85	1.82
3	11.83	11.39	3.75	9.41	8.02	14.78	3.34	2.04
4	11.52	11.28	2.12	8.99	7.78	13.40	3.42	1.91
5	10.83	10.43	3.73	8.19	7.09	13.34	3.65	1.81
6	10.57	10.35	2.06	7.82	6.91	11.65	3.75	1.71
7	11.59	11.25	2.94	9.10	7.78	14.51	3.38	1.92
8	11.31	11.15	1.39	8.78	7.58	13.73	3.51	1.81
9	11.87	11.16	6.04	7.20	6.74	6.81	6.06	1.33
10	11.77	11.31	3.91	7.06	6.71	5.19	6.16	1.27
11	12.89	12.32	4.44	8.38	7.71	8.69	5.83	1.46
12	12.77	12.40	2.92	8.01	7.58	5.69	6.03	1.38
13	11.80	11.41	3.33	7.17	6.73	6.56	6.22	1.26
14	11.57	11.32	2.16	6.85	6.59	3.81	6.29	1.21
15	12.65	12.31	2.73	8.12	7.54	7.64	5.90	1.39
16	12.54	12.38	1.21	7.90	7.44	6.21	5.99	1.32

Figs. 2.19 and 2.22):

1. compressor outlet and discharge line inlet ($P1$),
2. discharge line outlet and gascooler inlet ($P2$),
3. gascooler outlet and high-pressure-side internal heat exchanger inlet ($P3$),
4. high-pressure-side internal heat exchanger outlet and throttling valve inlet ($P4$),
5. throttling valve outlet and evaporator inlet ($P5$),
6. evaporator outlet and low-pressure-side internal heat exchanger inlet ($P6$),
7. low-pressure-side internal heat exchanger outlet and compressor inlet ($P7$).

The experimental data in terms of pressure, temperature and specific enthalpy for

the cornerstones of the thermodynamic cycle are reported in Tab. 2.8 for runs $\#1-8$, in Tab. 2.9 for runs $\#9-16$ and in Tab. 2.10 for runs $\#17-24$ of the experimental design. It was not possible to repeat the experimental tests a number of times suitable for evaluating the statistical scattering due to experimental inaccuracies. For this reason, the previous data are not provided with their error bars, but at least the accuracy of the instrument was considered. Moreover it was not possible to ensure exactly the same refrigerant charge during all the experimental tests because of the leakage problems. This point will be discussed better in Chapter 5. In order to reduce the effects of the refrigerant charge on the measurements, the experimental procedure included a preliminary phase during which the refrigerant mass was carefully regulated in order to reproduce a fixed reference cycle. To reproduce the reference cycle means that the pressure and specific enthalpy values for the seven cornerstones ($P1-7$), shown in Figs. 2.19 and 2.22, differ from the reference values for less than 2%. Even though this way of tuning the refrigerant charge is indirect, it allowed to verify the unperturbated reference cycle before investigating each test of the experimental plan.

Taking into account the previous data, it is possible to calculate the cooling capacity, the rejected thermal power and the TCOP for each experimental run. Since both air circuits are provided with temperature transducers (the effects due to moisture content can be neglected), it is possible to verify the thermal balance for both main heat exchangers. The post-processed experimental results are reported in Tab. 2.11. The difference between air-side and refrigerant-side measurements with regard to transferred thermal power are very good for the gascooler. In this case, the relative error on the thermal balance is less than 6%. Unfortunately the same error for the evaporator is much higher and it can be equal to 15% as maximum value. This error is not due to the simplifying assumption of neglecting the latent thermal power. In

fact this error means that the air-side estimation overestimates the transferred thermal power. Since only the sensible thermal power is measured, at most the air-side estimation should be smaller than refrigerant-side one, which involves both sensible and latent thermal power. Moreover the error is a monotonic increasing function of the air mass flow rate at the evaporator: the average error is around 6% for 0.27 kg/s and 13% for 0.33 kg/s. On the other hand, the refrigerant-side measurements for the evaporator are quite critical because, for all the experimental runs, a two-phase flow exists at the evaporator inlet and, for the majority of the experimental runs, the same holds at the evaporator outlet too. In this case, temperature and pressure data do not allow us to estimate the inlet and outlet void fraction. Hence the refrigerant-side measurements for the evaporator are indirect. The evaporator inlet enthalpy is assumed equal to the throttling valve inlet enthalpy and the evaporator outlet is estimated by means of the outlet enthalpy of the low-pressure-side internal heat exchanger and an extrapolated efficiency (95%) for the last component. The extrapolated efficiency is based on experimental data for the internal heat exchanger only. Anyway, despite the inaccuracies of the refrigerant-side measurements, it is plausible to trust them more because the estimated maximum error is close to 10%, which is lower than that on thermal balance. For this reason, it is plausible to suppose that the error is mainly due to an air leakage in the evaporator air circuit (EAC) between the measurement section for the air mass flow rate and the evaporator inlet. This means that a slightly reduced fraction of the measured air mass flow rate really passes through the evaporator and it is involved in the heat transfer process.

In the derivation of the reduced model, only the refrigerant-side data will be considered. Anyway, the described procedure is general and it can be applied to multiple experimental designs in order to find statistically meaningful results.

2.4 Reduced model

In this section, a reduced mathematical model which interpolates the experimental data will be developed. In this case, the reduction technique is essentially a regression method (see Fig. 2.16).

2.4.1 Design of the reduced model

First of all, the physical quantities must be properly made dimensionless in order to reduce the round-off errors. Let us define $\eta = h/h_0$ the dimensionless enthalpy, $\pi = p/p_0$ the dimensionless pressure and $\sigma = G/G_0$ the dimensionless refrigerant mass flow rate. In the same way, we can proceed for the air-side quantities. Let us define $\theta = T_a/T_0$ the dimensionless air inlet temperature and $\varsigma = G_a/G_0$ the dimensionless mass flow rate. The subscript will identify the generic component, according to the nomenclature introduced in the previous section. The input data for the model are the following user-defined quantities: ς_u^e, ς_u^g, θ_u^e, θ_u^g, σ_u and $\pi_{4,\,u}$, which is the set point of the back-pressure throttling valve. The output data are the cooling capacity $\Phi_e = G_0\, h_0\, \sigma(\eta_6 - \eta_5)$, the rejected thermal power $\Phi_g = G_0\, h_0\, \sigma(\eta_2 - \eta_3)$, the high-pressure-side internal thermal power $\Phi_{rh} = G_0\, h_0\, \sigma(\eta_3 - \eta_4)$, the low-pressure-side internal thermal power $\Phi_{rl} = G_0\, h_0\, \sigma(\eta_7 - \eta_6)$, the thermal power waste of the discharge line $\Phi_d = G_0\, h_0\, \sigma(\eta_1 - \eta_2)$ and finally the TCOP, calculated by means of Eq. (2.1). As it is evident by looking at the previous definitions, the reduced model must predict the cornerstones of the thermodynamic cycle in order to properly calculate all the output data.

As previously discussed, for a given experimental design, it is possible to extract an experimental sub-design by considering a proper sub-set of factors. For example, let us

consider a generic component k, which is characterized by some factors with regard to air-side condition, and let us suppose to keep them constant. All the residual factors allow us to define a factorial sub-design, which requires N_k runs. Since the number of runs for the experimental sub-design is smaller than that for full experimental design $N_k \leq N$, then $M_k = N/N_k$ multiple sub-designs exist. It is possible to use the results due to different sub-designs in order to statistically estimate the effects of the factors kept constant for each sub-design. If the component does not involve air circuits and there is no need to characterize the air-side condition, then $N_k = N$ and $M_k = 1$.

The enthalpy difference and the pressure difference for the generic k component contained between the cornerstone i and the cornerstone $i+1$ can be approximated as linear combinations of the inlet state i and the refrigerant mass flow rate, namely:

$$\eta_i - \eta_{i+1} = \alpha_\eta^k \eta_i + \alpha_\pi^k \pi_i + \alpha_\sigma^k \sigma^u + \alpha_0^k, \tag{2.3}$$

$$\pi_i - \pi_{i+1} = \beta_\eta^k \eta_i + \beta_\pi^k \pi_i + \beta_\sigma^k \sigma^u + \beta_0^k, \tag{2.4}$$

where α_η^k, α_σ^k, α_0^k are the coefficients of the linear approximation for the enthalpy difference and similarly β_η^k, β_σ^k, β_0^k are the coefficients of the linear approximation for the pressure difference. These coefficients can be obtained by two recursive least square fittings of the experimental data.

In the following, only the coefficients for the enthalpy difference will be reported but it is easy to proceed in a similar way for the pressure difference. Some auxiliary coefficients will be derived by a first least square fitting of the experimental data for the generic m sub-design. This yields:

$$\alpha_\eta^{k,m} \sum_{n=1}^{N_k} (\eta_i^n)^2 + \alpha_\pi^{k,m} \sum_{n=1}^{N_k} \eta_i^n \pi_i^n + \alpha_\sigma^{k,m} \sum_{n=1}^{N_k} \eta_i^n \sigma \quad + \quad \alpha_0^{k,m} \sum_{n=1}^{N_k} \eta_i^n = \sum_{n=1}^{N_k} \eta_i^n \left(\eta_i^n - \eta_{i+1}^n\right), \tag{2.5}$$

$$\alpha_{\eta}^{k,\,m}\sum_{n=1}^{N_k}\pi_i^n\eta_i^n+\alpha_{\pi}^{k,\,m}\sum_{n=1}^{N_k}\left(\pi_i^n\right)^2+\alpha_{\sigma}^{k,\,m}\sum_{n=1}^{N_k}\pi_i^n\sigma \quad + \quad \alpha_0^{k,\,m}\sum_{n=1}^{N_k}\pi_i^n = \sum_{n=1}^{N_k}\pi_i^n\left(\eta_i^n-\eta_{i+1}^n\right), \quad (2.6)$$

$$\alpha_{\eta}^{k,\,m}\sum_{n=1}^{N_k}\sigma\eta_i^n+\alpha_{\pi}^{k,\,m}\sum_{n=1}^{N_k}\sigma\pi_i^n+\alpha_{\sigma}^{k,\,m}\sum_{n=1}^{N_k}\left(\sigma\right)^2 \quad + \quad \alpha_0^{k,\,m}\sum_{n=1}^{N_k}\sigma = \sum_{n=1}^{N_k}\sigma\left(\eta_i^n-\eta_{i+1}^n\right), \quad (2.7)$$

$$\alpha_{\eta}^{k,\,m}\sum_{n=1}^{N_k}\eta_i^n+\alpha_{\pi}^{k,\,m}\sum_{n=1}^{N_k}\pi_i^n+\alpha_{\sigma}^{k,\,m}\sum_{n=1}^{N_k}\sigma \quad + \quad \alpha_0^{k,\,m}N_k = \sum_{n=1}^{N_k}\left(\eta_i^n-\eta_{i+1}^n\right). \quad (2.8)$$

The previous equations define a linear system of equations in the variables $\alpha_{\eta}^{k,\,m}$, $\alpha_{\pi}^{k,\,m}$, $\alpha_{\sigma}^{k,\,m}$ and $\alpha_0^{k,\,m}$. It is easy to verify that the matrix involved in this system of equations is the Vandermonde's matrix, which is generally characterized by high condition numbers. For this reason, searching for a good solution of the previous system by means of iterative techniques can be quite difficult. However for the present application, the small number of variables and the small number of experimental data allowed to easily solve the system by means of a direct technique.

Therefore a second least square fitting is performed on the previous interpolation coefficients themselves by considering all the M_k experimental sub-designs. In this case, the interpolation variables are those needed to characterize the air-side conditions. In the following, only the procedure for the coefficient $\alpha_{\eta}^{k,\,m}$ is reported but the same must be performed for $\alpha_{\pi}^{k,\,m}$, $\alpha_{\sigma}^{k,\,m}$ and $\alpha_0^{k,\,m}$ too. This yields:

$$\gamma_{\varsigma,\,\eta}^k\sum_{m=1}^{M_k}\left(\varsigma_m^k\right)^2+\gamma_{\theta,\,\eta}^k\sum_{m=1}^{M_k}\varsigma_m^k\theta_m^k+\gamma_{0,\,\eta}^k\sum_{m=1}^{M_k}\varsigma_m^k=\sum_{m=1}^{M_k}\varsigma_m^k\alpha_{\eta}^{k,\,m}, \quad (2.9)$$

$$\gamma_{\varsigma,\,\eta}^k\sum_{m=1}^{M_k}\theta_m^k\varsigma_m^k+\gamma_{\theta,\,\eta}^k\sum_{m=1}^{M_k}\left(\theta_m^k\right)^2+\gamma_{0,\,\eta}^k\sum_{m=1}^{M_k}\theta_m^k=\sum_{m=1}^{M_k}\theta_m^k\alpha_{\eta}^{k,\,m}, \quad (2.10)$$

$$\gamma^k_{\varsigma,\,\eta}\sum_{m=1}^{M_k}\varsigma^k_m+\gamma^k_{\theta,\,\eta}\sum_{m=1}^{M_k}\theta^k_m+\gamma^k_{0,\,\eta}\,M_k=\sum_{m=1}^{M_k}\alpha^{k,\,m}_{\eta}. \tag{2.11}$$

The previous equations define a linear system of equations in the variables $\gamma^k_{\varsigma,\,\eta}$, $\gamma^k_{\theta,\,\eta}$ and $\gamma^k_{0,\,\eta}$. The matrix involved in this system of equations is again the Vandermonde's matrix, but the same simplifying conditions, which have been previously discussed, hold. Finally the interpolating coefficient α^k_η involved in Eq. (2.3) can be derived by considering the user-defined input data, namely:

$$\alpha^k_\eta=\gamma^k_{\varsigma,\,\eta}\,\varsigma^k_u+\gamma^k_{\theta,\,\eta}\,\theta^k_u+\gamma^k_{0,\,\eta}. \tag{2.12}$$

This means that a first set of the user-defined input data, i.e. ς^e_u, ς^g_u, θ^e_u and θ^g_u, are involved in the calculation of the interpolating coefficients for the evaporator and the gascooler. If the component does not involve air circuits and there is no need to characterize the air-side condition, then $\alpha^{k,\,m}_\eta=\alpha^k_\eta=\gamma^k_{0,\,\eta}$.

The Eqs. (2.3, 2.4) can be written for all the components and they finally define a linear system of equations, which allows us to calculate all the cornerstones and consequently the thermodynamic cycle. This system of equations is:

$$\left[\begin{array}{cc}\mathbf{A}_\eta & \mathbf{A}_\pi\\ \mathbf{B}_\eta & \mathbf{B}_\pi\end{array}\right]\left\{\begin{array}{c}\mathbf{x}_\eta\\ \mathbf{x}_\pi\end{array}\right\}+\left\{\begin{array}{c}\mathbf{x}^{\mathbf{0}}_\eta\\ \mathbf{x}^{\mathbf{0}}_\pi\end{array}\right\}=0, \tag{2.13}$$

where the previous vectors are:

$$\mathbf{x}_\eta=\left\{\eta_1,\ \eta_2,\ \eta_3,\ \eta_4,\ \eta_5,\ \eta_6,\ \eta_7\right\}^T, \tag{2.14}$$

$$\mathbf{x}_\pi=\left\{\pi_1,\ \pi_2,\ \pi_3,\ \pi_4,\ \pi_5,\ \pi_6,\ \pi_7\right\}^T, \tag{2.15}$$

$$\begin{aligned}\mathbf{x}^{\mathbf{0}}_\eta\ =\ &\left\{\alpha^d_\sigma\sigma^u+\alpha^d_0,\ \alpha^g_\sigma\sigma^u+\alpha^g_0,\ \alpha^{rh}_\sigma\sigma^u+\alpha^{rh}_0,\ 0,\right.\\ &\left.\alpha^e_\sigma\sigma^u+\alpha^e_0,\ \alpha^{rl}_\sigma\sigma^u+\alpha^{rl}_0,\ \alpha^c_\sigma\sigma^u+\alpha^c_0\right\}^T,\end{aligned} \tag{2.16}$$

$$\begin{aligned}\mathbf{x}^{\mathbf{0}}_\pi\ =\ &\left\{\beta^d_\sigma\sigma^u+\beta^d_0,\ \beta^g_\sigma\sigma^u+\beta^g_0,\ \beta^{rh}_\sigma\sigma^u+\beta^{rh}_0,\ \pi^u_4,\right.\\ &\left.\beta^e_\sigma\sigma^u+\beta^e_0,\ \beta^{rl}_\sigma\sigma^u+\beta^{rl}_0,\ \beta^c_\sigma\sigma^u+\beta^c_0\right\}^T,\end{aligned} \tag{2.17}$$

and the previous matrices are:

$$\mathbf{A}_\eta = \begin{bmatrix} \alpha_\eta^d - 1 & +1 & 0 & 0 & 0 & 0 & 0 \\ 0 & \alpha_\eta^g - 1 & +1 & 0 & 0 & 0 & 0 \\ 0 & 0 & -1 & +1 & 0 & \alpha_\eta^{rh} & 0 \\ 0 & 0 & 0 & -1 & +1 & 0 & 0 \\ 0 & 0 & 0 & 0 & \alpha_\eta^e - 1 & +1 & 0 \\ 0 & 0 & 0 & 0 & 0 & \alpha_\eta^{rl} - 1 & +1 \\ +1 & 0 & 0 & 0 & 0 & 0 & \alpha_\eta^c - 1 \end{bmatrix}, \tag{2.18}$$

$$\mathbf{A}_\pi = \begin{bmatrix} \alpha_\pi^d & 0 & 0 & 0 & 0 & 0 & 0 \\ 0 & \alpha_\pi^g & 0 & 0 & 0 & 0 & 0 \\ 0 & 0 & 0 & 0 & 0 & \alpha_\pi^{rh} & 0 \\ 0 & 0 & 0 & 0 & 0 & 0 & 0 \\ 0 & 0 & 0 & 0 & \alpha_\pi^e & 0 & 0 \\ 0 & 0 & 0 & 0 & 0 & \alpha_\pi^{rl} & 0 \\ 0 & 0 & 0 & 0 & 0 & 0 & \alpha_\pi^c \end{bmatrix}, \tag{2.19}$$

$$\mathbf{B}_\eta = \begin{bmatrix} \beta_\eta^d & 0 & 0 & 0 & 0 & 0 & 0 \\ 0 & \beta_\eta^g & 0 & 0 & 0 & 0 & 0 \\ 0 & 0 & 0 & 0 & 0 & \beta_\eta^{rh} & 0 \\ 0 & 0 & 0 & 0 & 0 & 0 & 0 \\ 0 & 0 & 0 & 0 & \beta_\eta^e & 0 & 0 \\ 0 & 0 & 0 & 0 & 0 & \beta_\eta^{rl} & 0 \\ 0 & 0 & 0 & 0 & 0 & 0 & \beta_\eta^c \end{bmatrix}, \tag{2.20}$$

$$\mathbf{B}_\pi = \begin{bmatrix} \beta_\pi^d - 1 & +1 & 0 & 0 & 0 & 0 & 0 \\ 0 & \beta_\pi^g - 1 & +1 & 0 & 0 & 0 & 0 \\ 0 & 0 & -1 & +1 & 0 & \beta_\pi^{rh} & 0 \\ 0 & 0 & 0 & -1 & 0 & 0 & 0 \\ 0 & 0 & 0 & 0 & \beta_\pi^e - 1 & +1 & 0 \\ 0 & 0 & 0 & 0 & 0 & \beta_\pi^{rl} - 1 & +1 \\ +1 & 0 & 0 & 0 & 0 & 0 & \beta_\pi^c - 1 \end{bmatrix}. \tag{2.21}$$

In order to define the previous system of equations, some simplifying hypotheses have been considered. The back-pressure throttling valve has been described in an idealized way by assuming $\eta_4 = \eta_3$ and $\pi_4 = \pi_{4,u}$. Moreover the interpolating expressions for the internal heat exchanger differ from the other components. Since the internal thermal powers on both sides are very similar to each other (they can differ for non-ideal insulation only), it is better that both of them are functions of the same variables. The efficiency of the internal heat exchanger highly depends on the nature (single-phase or two-phase) of the fluid flow in the low-pressure-side. Hence it is

better to use the inlet conditions for the low-pressure part for interpolating both the transformations (3-4 and 6-7) realized by the internal heat exchanger because, in this way, it is easier to take into account the fact that the low-pressure-side fluid flow is single-phase or two-phase. For this reason, the enthalpy and pressure difference for the high-pressure part are expressed as linear functions of the inlet conditions for the low-pressure part.

2.4.2 Numerical results

First of all, the numerical results due to the reduced model have been compared with the original experimental data in order to verify that the two recursive least square fittings do not affect the reliability of the predictions. The comparison is reported in Tab. 2.12 and it shows a very good match for the most important quantities. In fact the discrepancy between the experimental data and the numerical results is very small for the cooling capacity ($-4.0\ \% \leq R \leq +4.1\ \%$) and for the rejected thermal power ($-1.6\ \% \leq R \leq +3.6\ \%$), while it is a bit higher for the TCOP ($-9.5\ \% \leq R \leq +9.2\ \%$). The reason is due to the fact that the TCOP involves a ratio of estimated quantities and it is very sensitive to inaccuracies. The accuracy is also poor for the transferred thermal power due to the internal heat exchanger. In this case, it is difficult to accurately predict thermal powers which are much smaller that those due to the main heat exchangers. Anyway the effects on the whole device performances due to the last inaccurate estimation of the internal thermal power are very modest. Recalling that the numerical results are due to a simple data fitting, the comparison is reasonable and the reduced model will be used for analysing the effects due to the VCS installation strategy. The evaporator can be installed:

- after the mixing point (AM) between recirculated air taken from the cabin and the refrigerated air due to the 3WM-ACS (see sketched lines in Fig. 2.6) and

Table 2.12: Comparison between experimental and numerical results due to reduced model for the considered factorial design (see Table 2.7). For each thermal power, three values are reported which are respectively the experimental datum (E), the numerical result due to the reduced model (M) and the relative percentage error (R), defined as $R = (E - M)/M \times 100$.

	Thermal Power										
	Gascooler $[kW]$			Evaporator $[kW]$			Internal $[kW]$		TCOP $[-]$		
	E	M	R	E	M	R	E	M	E	M	R
1	10.45	10.54	0.9	7.27	7.06	-2.8	3.83	3.42	1.93	1.75	-9.5
2	10.46	10.84	3.6	7.13	7.19	0.8	3.85	2.34	1.82	1.71	-5.9
3	11.39	11.26	-1.1	8.02	7.80	-2.8	3.34	3.30	2.04	1.93	-5.4
4	11.28	11.35	0.7	7.78	7.66	-1.6	3.42	3.50	1.91	1.78	-6.6
5	10.43	10.71	2.7	7.09	7.16	0.9	3.65	2.51	1.81	1.74	-3.7
6	10.35	10.57	2.1	6.91	6.91	-0.0	3.75	2.42	1.71	1.64	-4.1
7	11.25	11.17	-0.7	7.78	7.58	-2.6	3.38	3.44	1.92	1.81	-5.7
8	11.15	11.01	-1.3	7.58	7.30	-3.7	3.51	3.30	1.81	1.69	-6.5
9	11.16	11.03	-1.1	6.74	6.65	-1.3	6.06	6.72	1.33	1.32	-1.0
10	11.31	11.52	1.8	6.71	6.98	4.1	6.16	6.08	1.27	1.34	5.6
11	12.32	12.15	-1.3	7.71	7.43	-3.6	5.83	7.31	1.46	1.37	-6.3
12	12.40	12.52	1.0	7.58	7.68	1.4	6.03	6.14	1.38	1.39	0.9
13	11.41	11.47	0.5	6.73	6.91	2.8	6.22	6.28	1.26	1.32	4.9
14	11.32	11.34	0.1	6.59	6.79	3.0	6.29	5.64	1.21	1.30	7.1
15	12.31	12.39	0.7	7.54	7.66	1.6	5.90	5.90	1.39	1.42	2.2
16	12.38	12.34	-0.4	7.44	7.47	0.3	5.99	5.27	1.32	1.34	1.9
17	10.75	10.85	0.9	7.91	7.78	-1.6	1.93	2.47	2.20	2.15	-2.1
18	10.73	10.89	1.5	7.55	7.76	2.8	1.99	2.06	2.01	2.11	5.0
19	11.73	11.57	-1.3	8.63	8.28	-4.0	1.43	2.27	2.29	2.16	-5.7
20	11.62	11.72	0.9	8.24	8.37	1.5	1.56	1.64	2.10	2.15	2.0
21	10.80	10.73	-0.6	7.52	7.70	2.3	1.87	1.95	1.98	2.16	9.0
22	10.69	10.56	-1.3	7.23	7.42	2.8	2.04	1.95	1.84	2.01	9.2
23	11.62	11.49	-1.1	8.25	8.16	-1.2	1.54	1.92	2.09	2.10	0.3
24	11.50	11.32	-1.6	7.96	7.87	-1.1	1.68	1.78	1.96	1.96	0.0

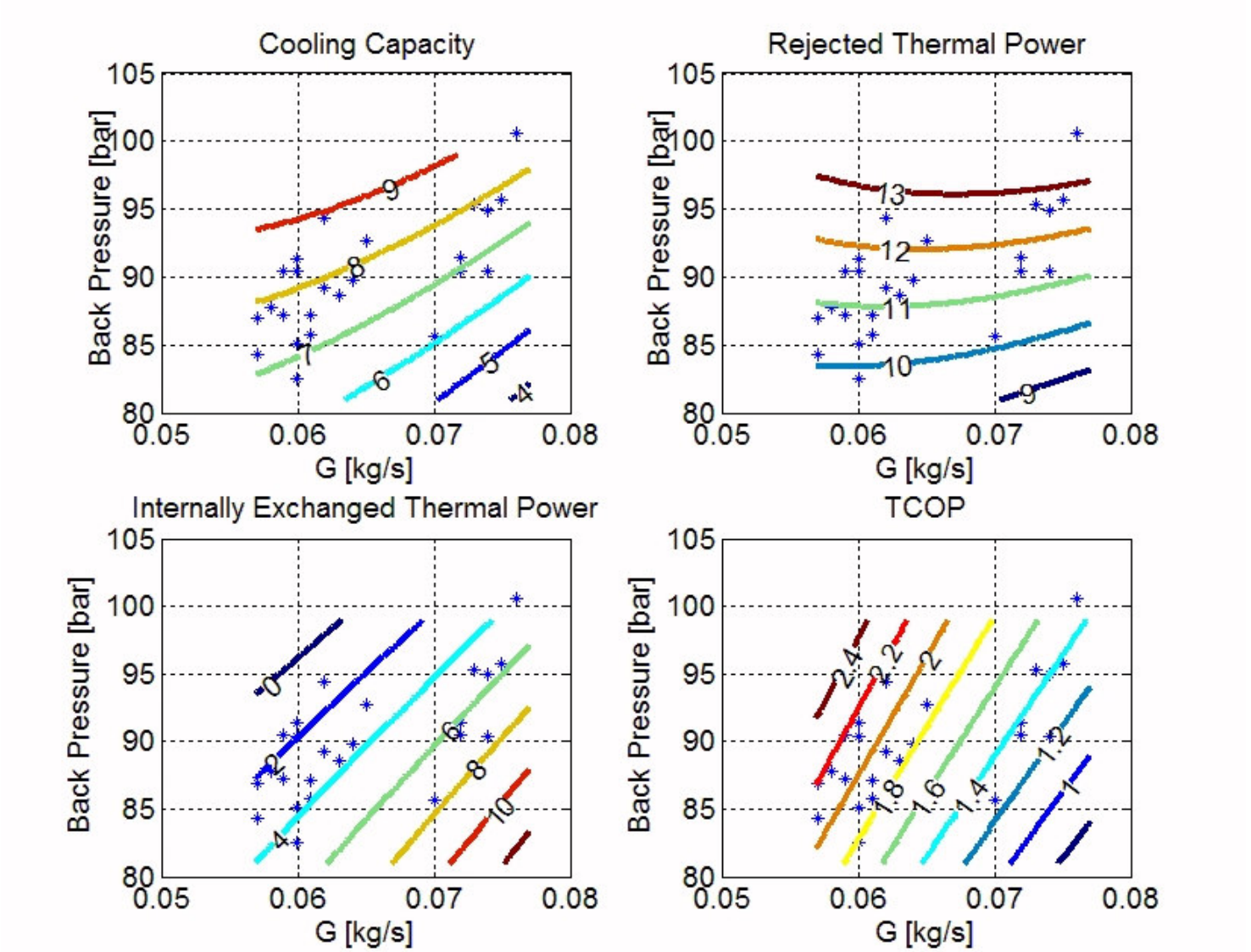

Figure 2.25: Numerical results due to reduced model: effects of refrigerant mass flow rate and set point of back-pressure valve with evaporator installed **after** the mixing point (see Fig. 2.6). The air-side conditions for the evaporator are $G_e = 0.47\ kg/s$ (maximum value) and $T_a^e = 20\ ℃$(minimum value), while those for the gascooler are $G_e = 0.30\ kg/s$ and $T_a^e = 27\ ℃$.

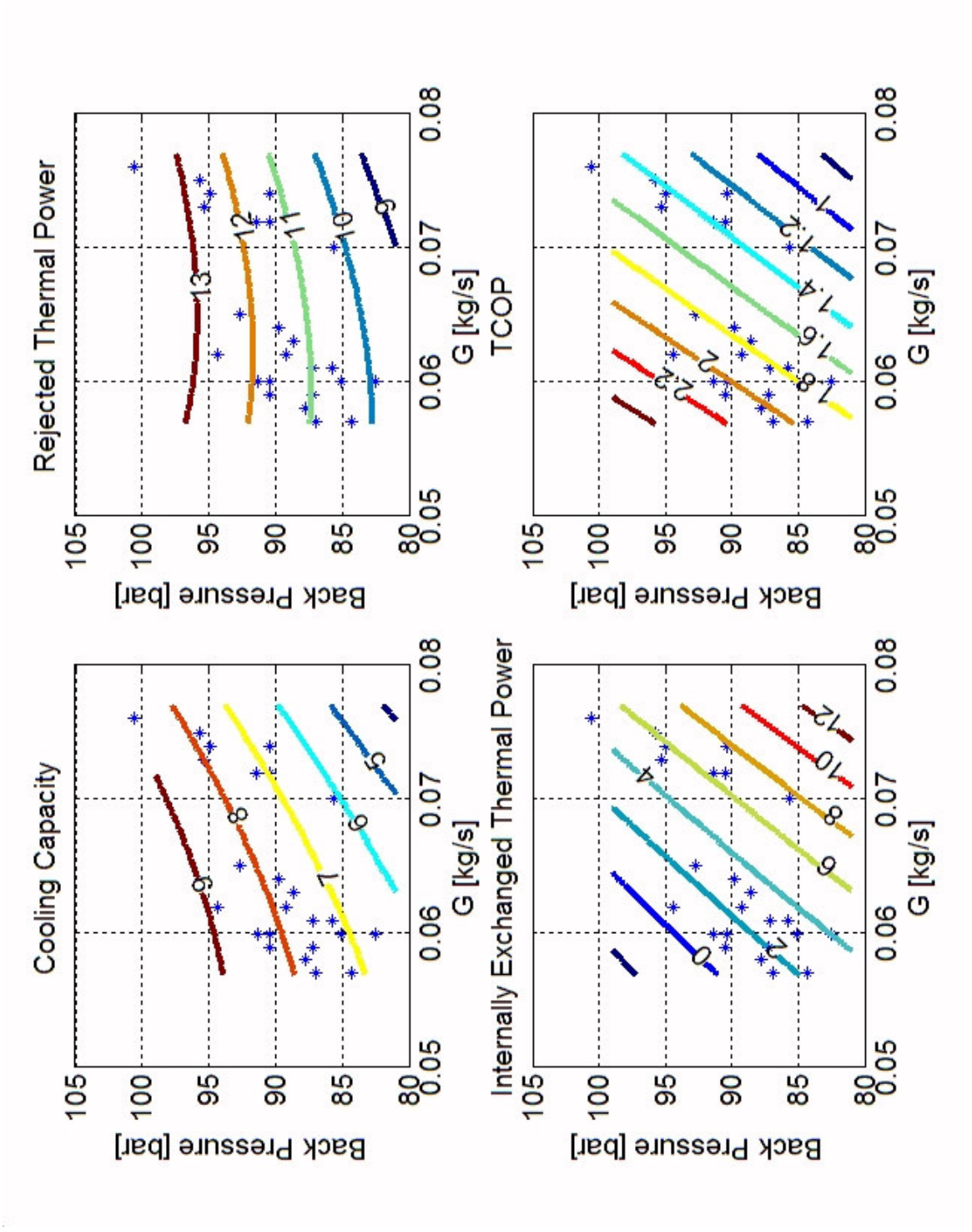

Figure 2.26: Numerical results due to reduced model: effects of refrigerant mass flow rate and set point of back-pressure valve with evaporator installed **before** the mixing point (see Fig. 2.6). The air-side conditions for the evaporator are $G_e = 0.27\ kg/s$ (minimum value) and $T_a^e = 30\ ^\circ C$(maximum value), while those for the gascooler are $G_e = 0.30\ kg/s$ and $T_a^e = 27\ ^\circ C$.

this would ensure the maximum air mass flow rate (roughly $G_a^e = 0.47\ kg/s$ for the low capacity tes rig) but the minimum air inlet temperature (roughly $T_a^e = 20\ ^\circ C$) or

- before the mixing point (BM) in the recirculation air duct which takes air from the cabin (see continuous lines in Fig. 2.6) and this would ensure the maximum air inlet temperature (roughly $T_a^e = 30\ ^\circ C$) but the minimum air mass flow rate (roughly $G_a^e = 0.27\ kg/s$ for the low capacity test rig).

Both previous configurations have been investigated and the numerical results for the cooling capacity, the rejected thermal power, the internal thermal power and the TCOP are reported in Figs. 2.25 and 2.26. The asterisks denote the actual experimental measurements. The air-side conditions for the gascooler are the same in both cases. The effects of the refrigerant mass flow rate and the set point of the back-pressure valve are investigated too. It is easy to verify that the previous results are substantially identical for both configurations. This seems somehow to prove the idea that the two configurations are equivalent, but they are not. In fact, the real systems do not work with a fixed refrigerant mass flow rate. In the electrified aircraft architecture, the compressor will be powered by an electrical motor controlled by an inverter and the feedback will be on the rotational speed. For this reason, the effective refrigerant mass flow rate can change according to the density of the actual suction condition. The same holds for the reported experimental design. Considering Tabs. 2.8, 2.9 and 2.10, it is easy to verify that the suction density decreases when the air mass flow rate at the evaporator increases. In fact, high air mass flow rate at the evaporator enhances the efficiency of the evaporator and consequently the super-heating too. Working with a fixed rotational speed leads to a consequent reduction of the refrigerant mass flow rate. As shown in the bottom-right sub-plots

of Figs. 2.25 and 2.26, reducing the refrigerant mass flow rate for a given set point of the back-pressure valve increases the TCOP. Unfortunately, as shown in the top-left sub-plots in the same figures, this reduces the cooling capacity too. For this reason, the after-mixing (AM) installation strategy (see Fig. 2.6) for the evaporator is preferable for reducing the energy consumption, but this could force to consider larger heat exchangers. Actually the air mass flow rate at the evaporator does not directly affect the performances of the transcritical cycle but it reduces the suction density, consequently the refrigerant mass flow rate and this is enough to increase the coefficient of performance.

2.5 Conclusions

In this section, the main outlines for the design of an experimental test rig which enables us to characterize the thermal performances of a refrigerating device based on a carbon dioxide transcritical cycle have been discussed. The final goal of this experimental test rig is to prove that the trascritical device can properly match the required specifications in order to be integrated with a conventional air-cycle machine and to realize in this way a hybrid air conditioning system for airborne application.

The experimental results are encouraging because the expected performances have been realized. This means that, in principle, the transcritical thermodynamic cycle can properly work for this application. However from the technological point of view, some problems still remain. First of all, the leakage problems of this prototype, which complicated the management of the experimental tests because they did not allow us to work with the same carbon dioxide charge for the whole experimental plan, would be completely unacceptable for a standard market device. Obviously this problem can be mitigated by considering better technologies for the gaskets, but this could

complicate the installation/maintenance of these devices in comparison with usual air-cycle machines. Secondly, automotive prototypes have been considered as components for the discussed exercise, but they are not the more lightweight and ultra-compact solutions, as required by airborne standards. Large opportunities of optimization in this direction exist, particularly for the compressor. Even though some compressors designed for other applications dealing with higher pressures exist (see, for example, methane compressors used in automotive applications, which are characterized by discharge pressures up to 200 bar), up to now the lubricants for carbon dioxide are still in their infancy and this substantially hinders the development of reliable carbon dioxide compressors.

Discussing the design of the experimental test rig, the importance of the thermal rejection phase for improving the performances of the transcritical cycle has been pointed out and consequently the importance of the gascooler too. Finned compact gascoolers made of flat extruded aluminum tubes with internal mini/micro-channels constitute a promising technology and the optimization of this type of heat exchangers is therefore one of the main research goal for the development of refrigerating systems operated with carbon dioxide. For this reason, these compact heat exchangers will be analyzed more extensively in the next chapter.